



BRNO UNIVERSITY OF TECHNOLOGY VYSOKÉ UČENÍ TECHNICKÉ V BRNĚ

CENTRAL EUROPEAN INSTITUTE OF TECHNOLOGY STŘEDOEVROPSKÝ TECHNOLOGICKÝ INSTITUT

DIGITAL PCR DEVELOPMENTVÝVOJ SYSTÉMU PRO DIGITÁLNÍ PCR

SUMMARY OF DOCTORAL THESIS

TEZE DIZERTAČNÍ PRÁCE

AUTHOR Ing. Martina Gaňová

AUTOR PRÁCE

SUPERVISOR prof. Ing. Pavel Neužil, Dr., DSc.

VEDOUCÍ PRÁCE

BRNO 2022

Abstract

In recent years, microtechnological and nanotechnological methods have proven to be a powerful analytical tools for deoxyribonucleic acid (DNA) analysis. There are reviewed different techniques developed over the last decade to amplify the nucleic acids (NA), including microfluidic systems. Polymerase chain reaction (PCR) is widely used in molecular biology to amplify target NA *in vitro*. The number of groups working on PCR worldwide is significant given the substantial social and economic impact of this technique, for example, in medical diagnostic, criminology, food processing, or environmental studies. Nowadays, the coronavirus disease 2019 pandemic proved the importance of developing more accessible technologies for diagnosing viral diseases.

The thesis presents the development of two versions of PCR platforms for NA detection, droplet real-time quantitative PCR (qPCR) and digital PCR (dPCR). The critical components of both platforms were fabricated using the microtechnological procedures for surfaces modification and lithographic fabrication, allowing the development of hydrophobic cover glasses or silicon microchips. The results of the thesis demonstrate the design, assembly, and testing with optimization of both platforms. The PCR technology consists of a software part controlled by the LabView program and a hardware part consisting of a temperature control system and a fluorescence imaging system. The droplet qPCR was conducted in 0.3 μ L of the master mix droplet containing the target gene encapsulated with 2 μ L of mineral oil. The droplets were pipetted on the hydrophobic cover glass, placed on the thermoelectric cooler (TEC) under the fluorescence microscope to conduct thermal cycling. The fluorescence changes during thermal cycling were captured by photomultiplier tubes and monitored by oscilloscope. The results of the testing also present the multiplexing capability of the developed technique. Three synthetic genes using intercalating fluorescent dye for simultaneous detection and quantification based on a single fluorescence channel were introduced. The droplet qPCR technology was a crucial platform for further development of the dPCR platform.

The dPCR platform employed a silicon microchip with microwell sample dispersion to the 26 448 microwells, each with a target diameter of 50 µm and a volume of 59 pL. The microchip loaded with the master mix containing the target DNA was covered by the mineral oil and cover glass modified by polydimethylsiloxane and Parylene C. The heating/cooling system of thermal cycling with the TEC was similar to the droplet qPCR platform. The fluorescent imaging system used a complementary metal-oxide-semiconductor (known as CMOS) camera to capture the fluorescent images. The developed dPCR was demonstrated for applications in human medical research. The synthetic virus DNA, isolated virus DNA, and female genomic DNA were tested. The thesis reveals the development of the dPCR system, which is a part of a new dPCR technique that is more affordable, easy to use with simple sample delivery, which are the most common problems why it has not yet found much popularity among laboratories. The silicon-based microchip dPCR improved the system performance due to a large number of wells. The employment of such dPCR benefits of high sensitivity, low signal to noise ratio, accuracy or lower detection limit, and multiplexing capability.

Keywords

Droplet qPCR, dPCR, thermal cycling, fluorescence detection, microtechnology, nucleic acids analysis, DNA amplification, melting curve analysis.

Abstrakt

Mikrotechnologické a nanotechnologické metody se v posledních letech ukázaly jako účinný nástroj pro analýzu deoxyribonukleové kyseliny (DNA). Různé techniky vyvinuté k amplifikaci nukleových kyselin (NK) byli publikovány v posledním desetiletí, včetně mikrofluidních systémů. Polymerázová řetězová reakce (PCR) je v molekulární biologii široce používána k amplifikaci cílové NK *in vitro*. Počet skupin pracujících s PCR po celém světě je obrovský vzhledem k důležitému sociálnímu a ekonomickému dopadu této techniky, například v oblasti lékařské diagnostiky, kriminalistiky, zpracování potravin nebo environmentálních studií. V současné době pandemie koronavirového onemocnění 2019 se prokázala důležitost vývoje přístupnějších technologií pro diagnostiku virových onemocnění.

Disertační práce popisuje vývoj dvou verzí platforem PCR pro detekci NK, kapkovou kvantitativní PCR v reálném čase (qPCR) a digitální PCR (dPCR). Klíčové komponenty obou platforem byly vyrobeny pomocí mikrotechnologických postupů pro úpravu povrchů a litografickou výrobu umožňující vývoj hydrofobních krycích skel nebo křemíkových mikročipů. Výsledky práce demonstrují návrh, sestavení a testování včetně optimalizace obou platforem. Technologie PCR je tvořena softwarovou částí, ovládanou programem LabView a hardwarovou častí sestávající ze systému řízení teploty a zobrazovacího systém florescence. Kapková qPCR byla prováděna v 0.3 µL kapky směsi obsahující cílový gen napipetovaný v objemu 2 µL kapky minerálního oleje. Kapky byly pipetovány na hydrofobní krycí sklo, které bylo umístěno na termoelektrický chladič (TEC) pod fluorescenční mikroskop, aby se provedlo teplotní cyklování. Změny fluorescence během cyklů byly zachyceny fotonásobičem a sledovány osciloskopem. Výsledky testování popisují také schopnost multiplexování vyvinuté techniky. V práci je představená amplifikace tří syntetických genů s využitím interkalačního fluorescenčního barviva pro simultánní detekci a kvantifikaci na základě jednoho fluorescenčního kanálu. Kapková technologie qPCR byla zásadní platformou pro další vývoj platformy dPCR.

Platforma dPCR používá křemíkový mikročip s disperzí vzorku do mikrojamek o celkovém počtu 26 448, každá s průměrem 50 µm a objemem 59 pL. Mikročip naplněn vzorkem byl pokryt minerálním olejem a krycím sklem modifikovaným polydimethylsiloxanem a Parylenem C. Systém ohřevu/chlazení teplotního cyklování s TEC byl podobný jako u kapkové platformy qPCR. Fluorescenční zobrazovací systém používal k zachycení fluorescenčních obrazů polovodičovou kameru na bázi CMOS. Vyvinutá dPCR byla testována pro aplikace ve výzkumu humánní medicíny. Testovací vzorky DNA byly část syntetického genu viru, izolovaná genomická DNA viru a izolovaná genomická DNA ženy. Diplomová práce popisuje vývoj systému dPCR, který je součástí nové techniky dPCR, která je cenově dostupnější a snadno použitelná s jednoduchým dávkováním vzorků, což jsou nejčastější problémy, proč si zatím mezi laboratořemi nenašla velkou popularitu. dPCR mikročip na bázi křemíku zlepšil výkon systému díky velkému počtu mikrojamek. Využití technologie dPCR vyniká ve vysoké citlivosti, v nízkém poměru signálu k šumu, dosahované přesnosti, v nízkém detekčním limitu a schopnosti multiplexování.

Klíčová slova

Kapková qPCR, dPCR, teplotní cyklování, detekce fluorescence, mikrotechnologie, analýza nukleových kyselin, amplifikace DNA, analýza křivky tání.

Bibliographic citation

GAŇOVÁ, Martina. *Digital PCR development*. Brno, 2022. Dissertation thesis. Brno University of Technology, Central European Institute of Technology BUT. Supervisor Pavel Neužil. Available from: https://www.vutbr.cz/studenti/zav-prace/detail/142708.

Declaration

I declare that I am the author of the doctoral thesis "Digital PCR development," and the presented work in the thesis was performed independently under the supervision of prof. Pavel Neužil, DSc. All technical literature and other information sources presented in this work are correctly cited in the text and listed in the reference list.

Brno, 01st March 2022	
	Ing. Martina Gaňová, author

Acknowledgments

I want to thank my supervisor, prof. Pavel Neužil, DSc. for his practical methodological and scientific support and other valuable advice during work on my thesis. I would like to thank my colleagues Ing. Tomáš Lednický, Ph.D., for technical support at PCR devices and LabView software and Ing. Peter Fecko for help and advice with microchip fabrication.

My thanks also to colleagues from Northwestern Polytechnical University (NPU) in China, Haoqing Zhang, for help and collaboration in sharing his knowledge and experience in the droplet and digital PCR during my doctoral studies and internship and to Zhiqiang Yan for support at MATLAB software.

I would like to express my sincere gratitude to all the people from different institutions who allowed me to measure on their instruments, provided samples for measurement or the consultation of the results. Namely, it's my friends from the faculty of Chemistry, cooperation with GeneProof company and prof. Marie Korabečná, Ph.D. from Charles University.

Table of contents

Abstract	3
Abstrakt	4
Introduction	7
Aims of the doctoral thesis	9
1 Development and validation of a droplet qPCR	10
1.1 Results and discussion	10
1.1.1 Droplet qPCR applications and multiplexing	10
1.1.1.1 Single gene qPCR amplification	11
1.1.1.2 PCR multiplexing based on a single fluorescent channel using dynamic MCA	
(published in [18])	12
1.2 Summary	15
2 Development and validation of a cdPCR	16
2.1 Results and discussion	16
2.1.1 Design and fabrication of microfluidic silicon chip for dPCR	17
2.1.2 Parylene C deposition protocol of cover glass for dPCR	19
2.1.3 cdPCR applications and multiplexing	20
2.1.3.1 The microwell chip sample loading optimization	20
2.1.3.2 Temperature non-uniformity detection on dPCR chips (published in [41])	21
2.1.3.3 Single gene dPCR amplification	25
2.1.3.4 PCR multiplexing based on a single fluorescent channel	32
2.2 Summary	35
1.1.1 Droplet qPCR applications and multiplexing 1.1.1.1 Single gene qPCR amplification. 1.1.1.2 PCR multiplexing based on a single fluorescent channel using dynamic MCA (published in [18]) 1.2 Summary. 2 Development and validation of a cdPCR. 2.1 Results and discussion. 2.1.1 Design and fabrication of microfluidic silicon chip for dPCR. 2.1.2 Parylene C deposition protocol of cover glass for dPCR. 2.1.3 cdPCR applications and multiplexing. 2.1.3.1 The microwell chip sample loading optimization. 2.1.3.2 Temperature non-uniformity detection on dPCR chips (published in [41]). 2.1.3.3 Single gene dPCR amplification. 2.1.3.4 PCR multiplexing based on a single fluorescent channel.	36
References	37
Dublications	40

Introduction

The biomacromolecules found in living organisms that carry genetic information are nucleic acids (NA), which include deoxyribonucleic acid (DNA) and ribonucleic acid (RNA) [1]. The molecular diagnostics offers various NA-based detection methods. The diagnostic industry, having recognized the benefits of NA testing, is investigating heavily in molecular biology research and development.

Polymerase chain reaction (PCR) dominates the NA amplification technology for detecting and quantifying the low concentration of NA [2]. Since its invention in the 1980s [3], PCR has found widespread applications in medical diagnosis, environmental monitoring, and food safety analysis [4]. Recently in 1999 has been developed a new generation of PCR called digital PCR (dPCR) [5]. It allows direct, reproducible, and accurate absolute quantification of target DNA without a standard [6]. Although several dPCR systems are commercially available, they are expensive and rarely used in local clinics. The expected rapid development of multiplex assays will improve the dPCR features, increase measurement capabilities, and decrease overall capital cost. However, current commercial dPCR technologies do not fulfil all these requirements, and therefore there is an interest in further technological improvements of these systems. Generally, the deployment of microfluidic technology and microfabrication could contribute to better possibilities of multiplexing. The following paragraphs are taken and reproduced from the review article [7].

Perspectives of PCR

The PCR systems are expected to play a notable role in the healthcare system to secure a better quality of life for the next generations. The global molecular diagnostics market size has been analyzed previously, where the PCR segment dominated the market. The market was valued at USD 36.2 billion in 2020 and is expected to expand at a compound annual growth rate of 3.9% from 2021 to 2028 [8]. Therefore, the fabrication of the new generation of PCR systems requires the deployment of advanced techniques and concepts that allow high-performance measurements and low power consumption to be integrated into portable miniaturized systems.

These new characteristics could facilitate the approach of such systems into small clinics or even doctor's surgeries, for example, PCR platform integrated into portable devices, such as smartphones. Such technology could allow physicians to monitor the disease and improve the healing rate of the patients. Portable nucleic acid analysis can be improved by forming an Internet of things (IoT). IoT is a network of communicating sensors or devices speaking with each other via the Internet to achieve intelligent identification, positioning, tracking, monitoring, and management. This technology can be integrated with point-of-care (POC) devices to speed up the information transfer from devices to the data center and then draw up a plan for the next step based on big-data analysis. If all the multiplexing dPCR devices for disease diagnosis are connected via IoT technology, the disease center can detect disease immediately and track the morbidity [7, 9].

Several portable miniaturized systems have been introduced in review *Multiplex polymerase chain reaction as a powerful diagnostic tool* [7]. These have been used to perform PCR for complementary DNA (cDNA) of the H7N9 avian influenza [10], reverse transcription PCR (RT-PCR) for RNA analysis of the H5N1 avian influenza [11], and the RNA of the Ebola virus [12].

The COVID-19 outbreak has accelerated the development of a simple sample-to-answer quantitative PCR (qPCR) [13, 14] and led to the converting of the ID NOW real-time loop-mediated isothermal amplification system [15] from influenza into a SARS-CoV-2 diagnostic tool, with other companies following suit. These developments should lead to systems being available for small clinics, with the precaution that the sample is placed in a sealed cassette to avoid sample contamination and not harm the operators. Safe handling of the sample would eliminate the requirements of extensive laboratory biosafety measures and reduce costs.

DNA quantitative analysis using dPCR with high accuracy has already been proven. The combination of diagnostic PCR platforms and smartphones should result in POC applications as it has a detection system, and additional optical filters can be added at a low cost. A miniaturized dPCR platform has been reported [16] that uses a smartphone with an Android operating system (OS) to control the heater via Bluetooth and perform thermal cycling. The built-in phone camera captures the fluorescence image, and software in the Android OS manages the image analysis. The system can be expanded to perform multiplexed dPCR using intercalating dye and capture a sequence of fluorescent images at different temperatures [17].

Aims of the doctoral thesis

The doctoral thesis aimed to demonstrate the accessible dPCR technology that implements the simple operation of the device with new architecture, a surface treatment method, and a new sample loading method than currently available dPCR systems. The goal was to propose dPCR technology that will expand to the miniaturized and portable platform, thus enlarging its use in local clinics.

To overcome unexpected drawbacks, the development was divided into two main parts: (1) **development and validation of a droplet qPCR** with its detection system and subsequent (2) upgrade of droplet qPCR to the **dPCR system**. The research plan was divided into particular tasks starting with the key droplet qPCR development following dPCR chip fabrication with instrumentation, capturing the fluorescent image and its processing, as well as optimizing the dPCR method for applications.

Task 1 Instrumentation of droplet qPCR hardware: The amplification system consisted of a heating/cooling unit for thermal cycling using a thermoelectric cooler (TEC) element and the fluorescence detection system.

Task 2 Development of LabView software for temperature control: The proposed LabView-based temperature control program allowed to set the time and thermal cycling protocol of the droplet qPCR system to perform quantitative amplification of target gene. Later, the LabView temperature control program was used to control dPCR thermal cycling.

Task 3 Droplet qPCR applications and multiplexing: The qPCR was performed in a droplet consisting of a master mix with DNA templates, relevant primers, and other PCR components covered with mineral oil with the volume of $\approx 0.3~\mu L$ and $\approx 2.0~\mu L$, respectively. Then multiplexing was performed in the presence of an intercalating dye using the single fluorescent channel.

Task 4 Instrumentation of dPCR hardware: The dPCR technology for detection and quantification of nucleic acid using a silicon (Si) chip was demonstrated. The dPCR system employed a TEC element for heat up and cool down the system controlled by the LabView program (proposed in task 2) and the fluorescence detection system.

Task 5 dPCR image processing: The MATLAB environment for the digital processing of fluorescent images was used to perform a quantitative sample analysis.

Task 6 dPCR applications and multiplexing: The chip with wells was loaded with a master mix PCR solution containing the DNA template and then encapsulated with mineral oil and polydimethylsiloxane (PDMS) and Parylene C coated cover glass to prevent the evaporation of the sample. The spectrum of different samples mirroring different biological material was obtained allowing to explore the capabilities of the newly developed technology. Then multiplexing with one dPCR chip was performed in the presence of an intercalating dye using single fluorescent channel detection.

1 Development and validation of a droplet qPCR

The concentration of target NA in clinical samples is typically low, which is usually undetectable by most existing detection methods, hence necessitating the amplification process. Here, is proposed a PCR technique for NA detection; droplet qPCR to perform continuous fluorescence monitoring (CFM) method, providing qualitative and quantitative sample information. The technique was also applied for multiplex detection of hepatitis B virus (HBV), human immunodeficiency virus (HIV), and glyceraldehyde 3-phosphate dehydrogenase (GAPDH) genes in different concentration ratios.

The master mix with the target DNA molecules was emulsified into the mineral oil droplet. The thermal cycling was performed in the oil droplet, which served as a virtual reaction chamber (VRC) (Figure 1A, B). The results demonstrate the design, assembly, and testing with optimization of the droplet qPCR platform. The PCR running in a droplet was performed to test the hardware parts of the device together with the temperature control system. The technique was developed as a preliminary platform to overcome unexpected drawbacks during dPCR development, and it was a crucial platform for further improvement of the dPCR technique.

1.1 Results and discussion

The PCR technology consists of a software part controlled by the LabView program and a hardware part consisting of a temperature control system and a fluorescence imaging system (Figure 1C, D). The droplet qPCR was conducted in $0.3~\mu L$ of the master mix droplet containing the target gene encapsulated with $2~\mu L$ of mineral oil. The droplets were pipetted on the hydrophobic cover glass placed on the TEC under the fluorescence microscope to conduct thermal cycling.

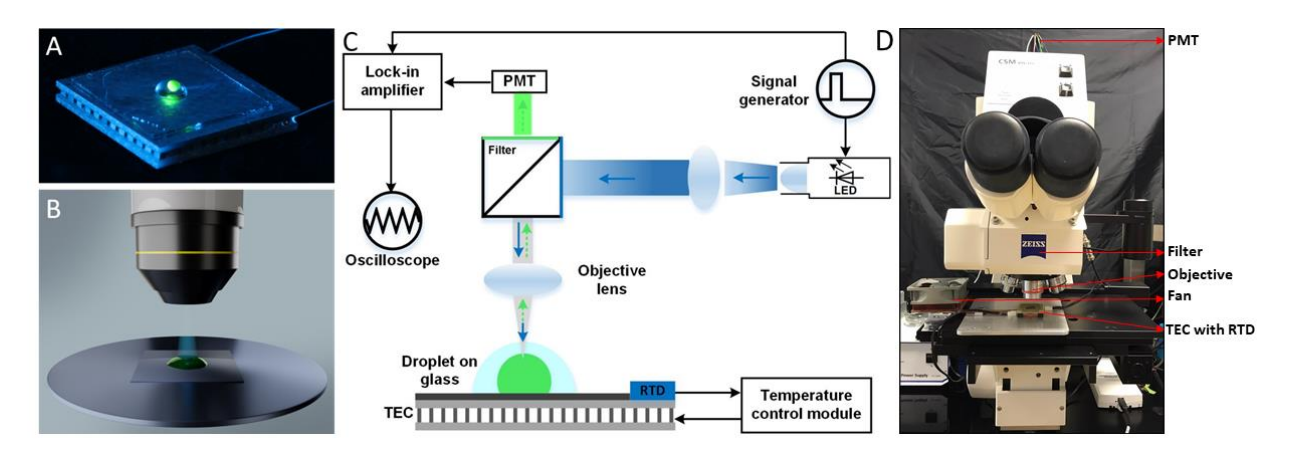


Figure 1 (A) Photograph of a VRC on a TEC with a droplet of fluorescein covered with mineral oil. (B) Schematic representation of the LED illuminated through an objective microscope lens. (C) Diagram of the testing setup. (D) Photograph of the droplet dPCR hardware. Figures A-C were reproduced from [18].

1.1.1 Droplet qPCR applications and multiplexing

The PCR has become a well-established method for detecting and amplifying DNA with a specific sequence. Incorporating fluorescent probes, known as TaqMan probes, or DNA intercalating dyes, such as SYBR Green, into the PCR mixture allows real-time monitoring of the reaction progress and extraction of quantitative information. Previously reported real-time PCR product detection using intercalating dyes required melting curve analysis (MCA) to be performed following thermal cycling.

Here, a technique is presented to perform dynamic MCA during each thermal cycle determining the PCR product specificity in real-time instead of waiting until the end of the PCR. The following parts 1.1.1.1 - 1.2 are reproduced from our publication [18].

1.1.1.1 Single gene qPCR amplification

The PCR master mix of HBV, HIV, and GAPDH was prepared and initially verified using a commercial PCR cycler to identify the respective values of critical threshold (C_T) and melting temperature (T_M) of amplicons; T_M for HIV, HBV, and GAPDH was ≈83.0, 87.5, and 79.0°C, respectively (data not shown). The same PCR protocol was then performed in a droplet on the TEC with a set temperature scan rate (ν) of 0.8 K·s⁻¹ from elongation to denaturation. The temperature (T) and fluorescence (T) signals were recorded for further processing.

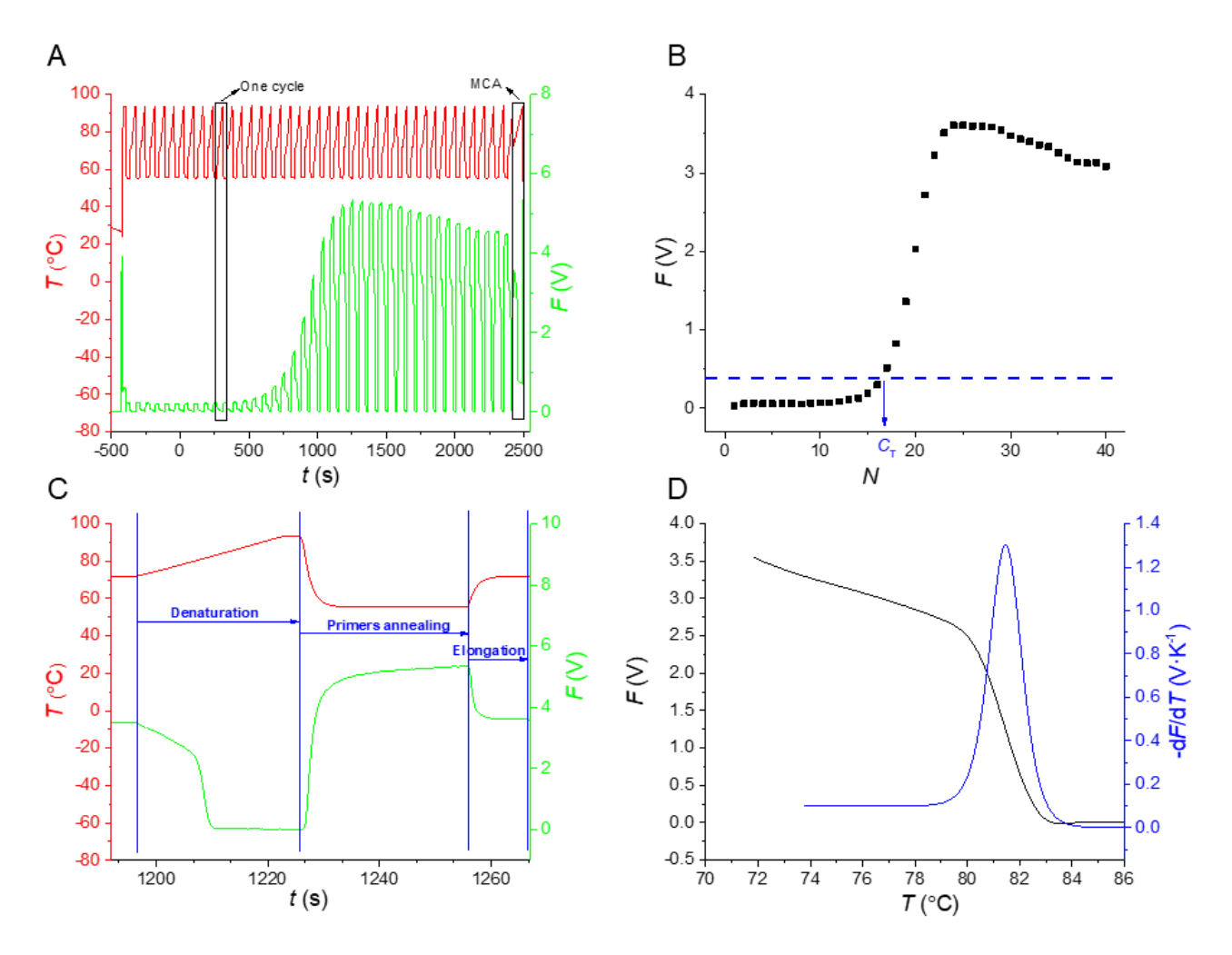


Figure 2 Droplet qPCR amplification of HIV gene. (A) Continuous fluorescence intensity (green) and heater temperature (red) from 40 cycles and MCA at the end of the PCR protocol. (B) The F values as a function of cycle number (N) and extracted C_T value. The F values were extracted at the end of the elongation step in each cycle from figure A, resulting in the amplification curve. (C) The detail of fluorescence intensity (green) and heater temperature (red) from 1 cycle. (D) MCA curve (black) recorded at the end of the PCR protocol and its derivative -dF/dT (blue) as a function of T. Reproduced and modified from [18].

The PCR protocol was performed based on a CFM method to monitor F (Figure 2A) as a function of time (t), concurrently recording the heater T (Figure 2A) [19]. The PCR experiment was performed with the HIV gene. The amplification curve was extracted (black squares in Figure 2B) from the PCR (Figure

2A) using the conventional approach of registering the F amplitude at the end of the extension phase in each PCR amplification cycle. The following way determined the C_T . The amplification curve was first fitted using nonlinear curve fitting and the function:

$$Y = a + b \cdot N^c, \tag{1}$$

where Y is the extracted signal data, either F or $\neg dF/dT$, and a, b, and c are fitting parameters. Then, we determined the C_{\top} values by solving Equation (2) using the formula:

$$C_{T} = 10^{\frac{\log \frac{Y_{T} - a}{b}}{c}}, \qquad (2)$$

where Y_T is the F value at the set value of C_T defined as 10% of the signal increase, either F or -dF/dT. The C_T value was ≈ 16.4 . The analysis of the fluorescence intensity (green) and heater temperature (red) from one cycle is shown in Figure 2C, and the cycle number is 23. The cycle consisted of three steps: denaturation, primers annealing, and elongation. The transition from the elongation to the denaturation step (from 72 up to 95°C) represents the MCA temperature range. Thus, it could serve for product specificity determination [18, 20]. At the end of thermal cycling, the MCA was performed (Figure 2A), and the details of the curve are shown in Figure 2D (black curve) with its derivative -dF/dT as functions of T (blue curve), determining the specificity and T_M of amplified products.

1.1.1.2 PCR multiplexing based on a single fluorescent channel using dynamic MCA (published in [18])

The following sections 1.1.1.2 - 1.2 are reproduced from [18]. Patients with acquired immunodeficiency syndrome are infected by HIV, thus weakening the human immune system in its fight against other diseases such as hepatitis B and tuberculosis. In HIV infected patients, HIV exacerbates the symptoms of HBV virus infection and accelerates the progression of the liver disease leading to cirrhosis as well as hepatocellular carcinoma. Disease progression to cirrhosis in HIV-positive patients is almost 3 times faster than in HIV-negative patients, and the interaction of HIV and HBV remains the leading cause of death [21-23]. Growing globalization and human migration have accelerated the spread of these diseases, and no country has been immune from them [24-26]. Therefore, it is essential to have early diagnosis and treatment of these diseases to lower death rates.

Here is presented the PCR experiment on the HIV gene only as an example of data extraction. The PCR protocol was performed based on a CFM method to monitor F (Figure 3A) as a function of t, concurrently recording the heater T (Figure 3A). The fluorescence signal F(t) and temperature T(t) registered during the transition from elongation to denaturation step (from 72 up to 95°C) were split in successive PCR cycles and plotted as a function of t with the PCR cycle number (N) as a parameter (Figure 3B). Then, the MCA was performed by eliminating t from F(t) and T(t), giving F and its derivative -dF/dT as functions of T (Figure 3C). Finally, the amplification curves (black squares in Figure 3D) were extracted from the PCR (Figure 3A) using the conventional approach of registering the F amplitude at the end of the extension phase in each PCR amplification cycle. Then, the peak value of -dF/dT as a function of N (red circles in Figure 3D) was plotted, resulting in a second amplification curve determined from MCA. Here, the C_T values determined from the PCR curve and MCA were ≈ 16.4 and 16.3 cycles,

respectively (Table 1), differing only by \approx 0.12 cycle, suggesting that these two methods of C_T extraction are equivalent.

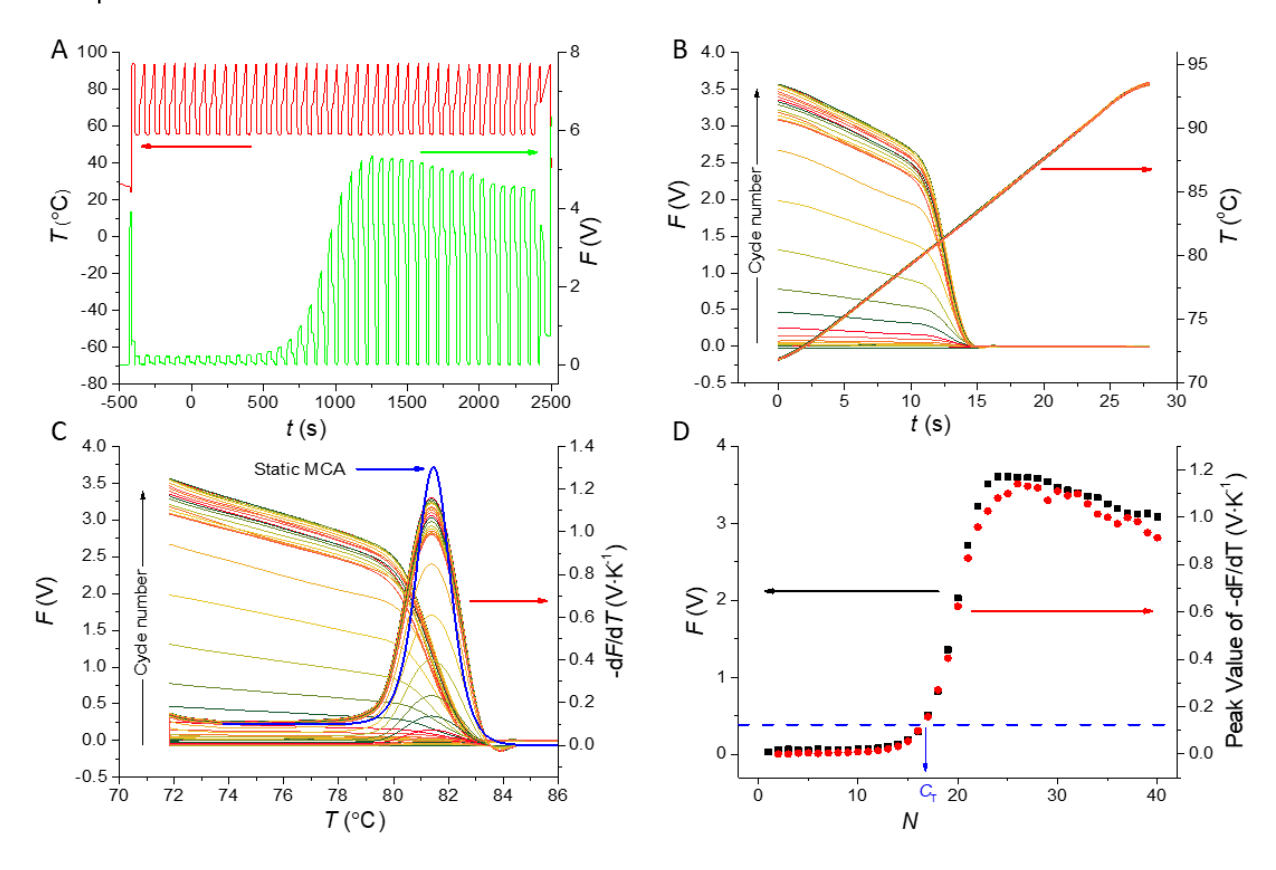


Figure 3 Principle of PCR data processing and extraction of PCR amplification curves. (A) Continuous fluorescence intensity (green) and heater temperature (red) from 40 PCR cycles. (B) Extracted F values from 72 up to 95°C (left Y axis) and T (right Y axis) as a function of t with N as a parameter. (C) MCAs (left Y axis) and its derivative -dF/dT (right Y axis) as a function of T with N as a parameter. The blue curve represents the static MCA recorded at the end of the PCR protocol. (D) Two amplification curves: the first (black squares) is the conventional extraction from figure A as the F value at the end of the elongation step; the second (red circles) is the peak values of -dF/dT at each cycle extracted from figure C. The extracted C_T values are shown. Reproduced from [18]

Subsequently, the combination of HIV, GAPDH, and HBV genes was amplified to demonstrate the multiplexing capability of the method. The combination of HIV with GAPDH was chosen in three different ratios; for the combination of all three, the GAPDH content was kept constant while the other two were varied (Table 1). Details of all processed data are published in the publication [18]. Here, the results for genes with a volume ratio of 5:5:5 are presented to demonstrate the multiplexing method. First, the PCR was performed with v set to 0.8 K·s⁻¹ while recording both T and F as a function of t, followed by MCA with v set to 0.1 K·s⁻¹ (Figure 4A). The data were recorded by an oscilloscope and then registered and processed with a MATLAB script, as described in the paragraph above. The F and T data from all cycles were split into individual cycles and plotted as a function of t (Figure 4B). Then, t was eliminated, and we plotted F and -dF/dT as a function of T, including the static MCA, extracted directly from Figure 4A (Figure 4C). There are three peaks corresponding to HIV, GAPDH, and HBV amplicons with respective $T_{\rm M}$ values compared to those extracted from static MCA. The difference between $T_{\rm M}$ of GAPDH and HIV is only ≈2.72°C, and the results are clearly differentiated, showing that their T_M difference could perhaps be significantly smaller. Then, it was plotted a composite PCR amplification curve using the F values at the end of the elongation steps (Figure 4A) and individual PCR amplification curves (Figure 4D) as peak values of respective genes from -dF/dT in Figure 4C. Finally, the C_T values were calculated by the

method described above. The experiments showed that the different DNA molecules during multiplex PCRs influenced each other as they competed for the same limited pool of component supplies, especially enzymes and nucleotides. The outcome was that the more efficiently amplified gene negatively affected the yield of other amplicons [27], changing their PCR amplification efficiency. The presented data processing method dynamically provided qualitative and quantitative information about the target genes in the sample and was confirmed for every volume ratio.

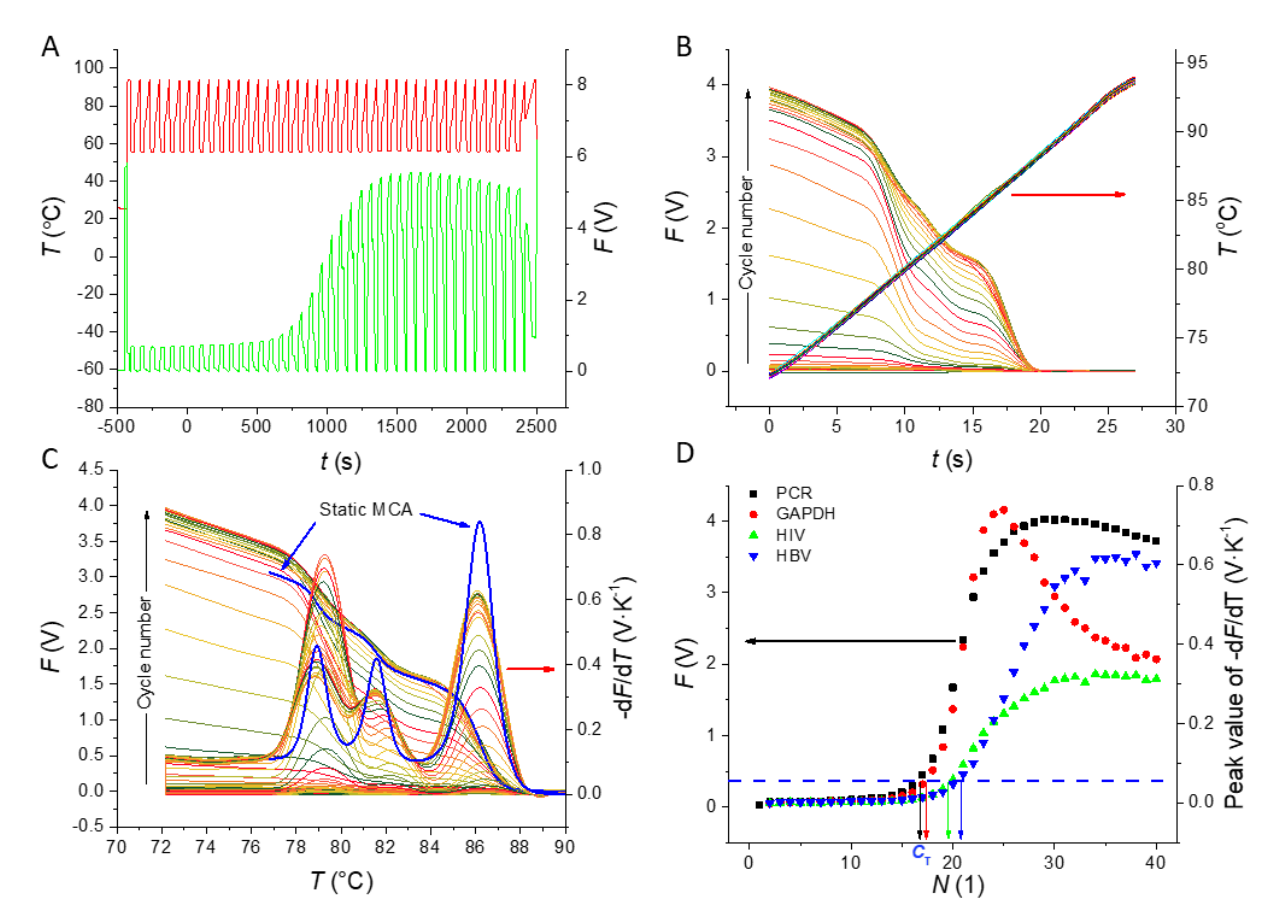


Figure 4 Dynamic MCA results from amplification of three genes. (A) Continuous fluorescence intensity (green) and heater temperature (red) from 40 PCR cycles. (B) Extracted data of T and fluorescence signal change from each cycle during the transition from the annealing to the denaturation temperature with a scan rate v set to 0.8 K·s⁻¹ as a function of time. (C) Split MCA curves F(T) and its derivative $\neg dF/dT(T)$ of each cycle as a function of temperature. The blue curves represent the result of static MCA recorded at the end of PCR amplification, and the static MCA reproduces the shape of the dynamic MCA. (D) Demultiplexed quantitative data represented by three amplification curves extracted from the peak values correspond to the three individual genes (red for GAPDH, green for HIV, and blue for HBV). The fourth amplification curve (black) is extracted from the PCR amplification (from figure A). The blue line is a baseline to extract a threshold cycle for every gene contained in the sample. Reproduced from [18].

qPCR multiplexing was developed to detect two or more specific nucleic acids in a single reaction primarily using TaqMan probes specific to each amplicon and having different color fluorophores [28]; it has been used to detect the presence of viruses [29] and pathogens [30], for species authentication [31], and for food safety [32]. This method requires hardware with multiple optical fluorescence channels and wide optical spectrum photodetectors using either photodiodes or photomultiplier tubes or a single-channel system utilizing a spectrum analyzer. A single fluorescent channel with a PMT has been used with a combination of a 6-carboxyfluorescein probe (FAM probe) and an intercalating dye [33] to extract the *F* amplitude in each PCR cycle twice, before and after DNA denaturation, resulting in two PCR amplification curves, effectively doubling the PCR throughput. Later, the experiments were extended and updated to determine the advantages and limitations of qPCR duplexing in a single fluorescent channel [34]. Intercalating dye-based end-point PCR multiplexing has also been shown to detect specific serotypes of *Vibrio cholerae* [35] or dengue fever viruses [36].

Table 1 Extracted values of C_T from standard PCR as well as from dynamic amplification curves. Reproduced from [18].

Expt. order	Volume ratio	HIV (C _T)	HBV (C _T)	GAPDH (C _T)	PCR (C _T)
1	10:0:0	16.29	N.A.	N.A.	16.41
2	0:10:0	N.A.	16.17	N.A.	14.60
3	0:0:10	N.A.	N.A.	15.81	14.45
4	1:0:1	19.91	N.A.	16.14	14.98
5	1:0:2	21.96	N.A.	16.13	14.95
6	2:0:1	18.65	N.A.	16.48	16.06
7	5:5:5	18.67	20.61	17.78	16.93
8	5:4:5	17.41	19.97	17.14	16.49
9	5:2.5:5	17.49	21.62	17.39	16.46
10	2.5:2.5:5	18.90	21.70	17.51	16.48

Alternatively, utilization of the CFM method [37] to capture hundreds of data points in each cycle allows the observation of PCR progress, including reaction kinetics, while providing both F and T as functions of time. Eliminating t during the transition from elongation to denaturation during PCR gives F as a function of T, i.e., MCA. This method was utilized to multiplex hemagglutinin and neuraminidase genes in avian influenza RNA virus, as well as to determine the original number of copies, using the intercalating EvaGreen dye [20] with an assumption that the $T_{\rm M}$ difference between two amplicons was at least 5°C. Unfortunately, the experimental data and the results of the multiplex qPCR processing method could not clearly differentiate peaks due to the high scanning rate of 20 K·s⁻¹ or more. The same technique of PCR multiplexing was used later for digital PCR [38]. Recently, a new method for multiplexing using intercalating dyes was proposed based on multidimensional standard curves [39, 40]. The data obtained by this novel method were achieved by commercial qPCR instruments, thus extending the use of these devices. Here the presented PCR multiplexing method is based on data extracted from MCA performed during each thermal cycle. The PCR uses the CFM method with one, two, and three genes in different volume ratios, demonstrating that 2°C difference in $T_{\rm M}$ of amplicons is sufficient to subsequently demultiplex quantitative data for individual genes. The proposed method allows researchers to detect multiple genes in real time and to decide whether to stop or optimize the experiment based on the real-time results. As a result, the process can be shortened and become more efficient.

1.2 Summary

A method of quantitative PCR multiplexing is based on performing melting curve analysis during each PCR cycle by controlling the ramping rate in the transition phase from elongation to denaturation. A single fluorescent channel with an optical wide-band detector, an intercalating dye, and different values of $T_{\rm M}$ for individual amplicons were used to verify the proposed method. The capability of this method was demonstrated by multiplexing up to three genes. PCR amplification curves for each gene were constructed, which can serve for the determination of the initial DNA concentration in the sample. Additionally, the lower transition rate set to 0.8 K·s⁻¹ from elongation to denaturation provides data used for multiplexing assay, which could also be used in genotyping. These advantages of simple single fluorescent channel multiplexing could inspire developers of new gPCR systems to enhance their

hardware and software capability to enable it. It would be a rather simple task for newly developed portable devices for rapid detection of infectious diseases outside of laboratories, in the field, and at the point of care. So they could contribute to help early diagnosis and treatment of HIV, HBV, and other viral diseases. These new multiplexed systems could also be connected to a global health system as part of the Internet of Things [9].

The developed droplet qPCR technique was verified by measurement, the drawbacks of hardware and software parts were eliminated, the methods and protocols were optimized. The achieved results present the utilization of the platform. This preliminary platform fulfilled its main purpose. Thus, the platform was further developed to the dPCR technique.

2 Development and validation of a cdPCR

Over the past few decades, the development of microfluidics has enabled new technologies such as dPCR. dPCR was originally developed to perform absolute DNA quantification of a sample. dPCR can also detect rare DNA sequences among a background of abundant ones. Here is introduced a chip dPCR technique to perform qualitative and quantitative sample analysis. The technique was also applied for multiplex detection of Chr21 and Chr18 genes.

The following section presents the designed dPCR configuration for NA detection; cdPCR with microwell sample dispersion. The master mix with the target DNA molecules was loaded to the small independent partitions. The partitions were covered by mineral oil and modified cover glass. The thermal cycling was performed in the silicon microchip. The dPCR amplification was accomplished to test the system's precision by amplifying target DNA with different copy numbers. Moreover, the multiplex assay was performed to determine the capability of the newly developed platform. Thus, the achieved results demonstrate the design, assembly, and testing with optimization of the dPCR platform.

2.1 Results and discussion

The dPCR technology consists of a software part controlled by the LabView program and a hardware part (Figure 5A) consisting of a temperature control system and a fluorescence imaging system (Figure 5B). The dPCR technology is similar to the droplet qPCR platform with few crucial differences. The cdPCR was conducted in microwell of volume 59 pL with a total number of microwells 26 448. The whole surface of the silicon chip was covered by 10 μ L of mineral oil and modified cover glass. The loaded chip with the sample was placed on the TEC under the objective camera lens to conduct thermal cycling (Figure 5C, D).

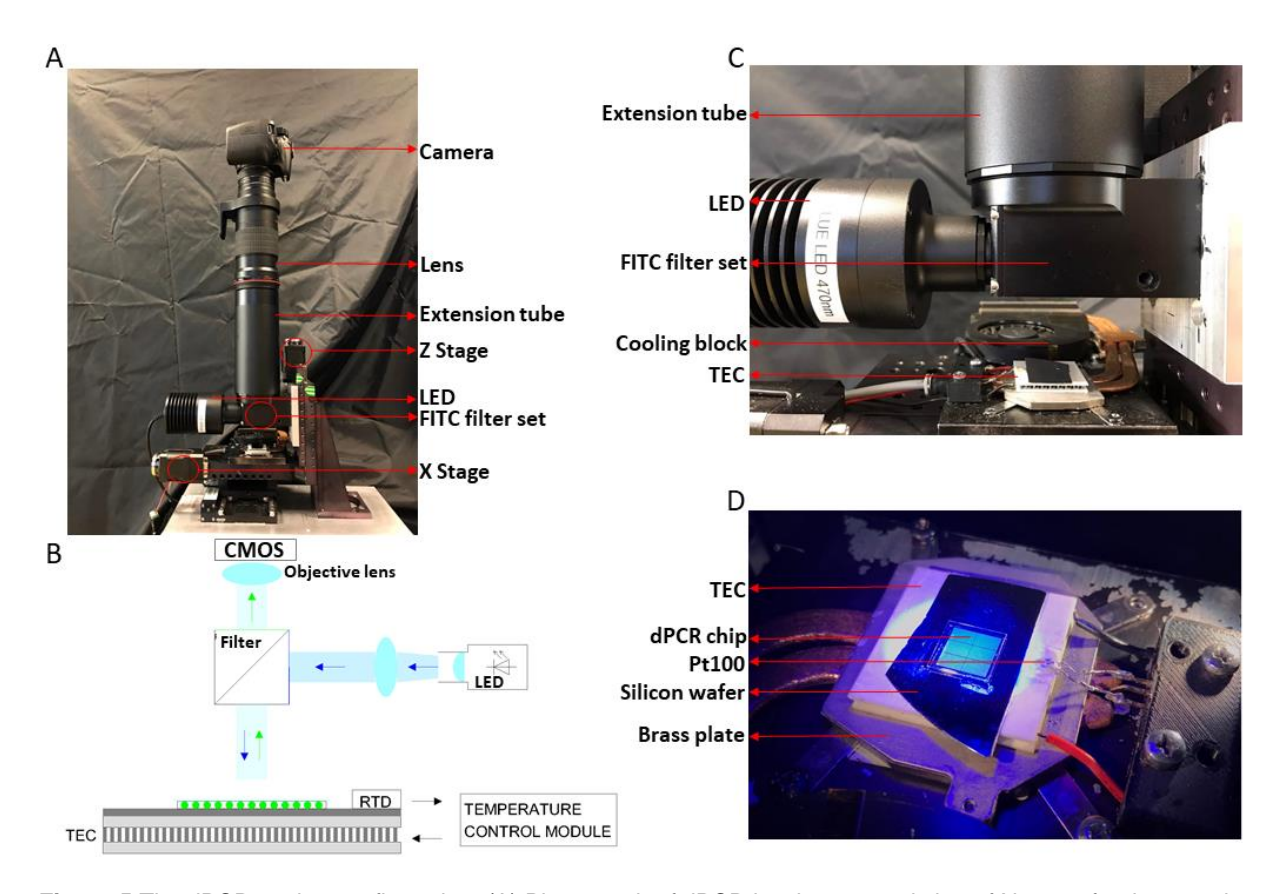


Figure 5 The dPCR testing configuration. (A) Photograph of dPCR hardware consisting of X-stage for the sample, including TEC and temperature sensor Pt100. The sample is illuminated via the fluorescent cube by a light-emitting diode (LED). A camera captures a fluorescent image of the chip via a spacer tube, macro lens, and a 1.4× extension. (B) Diagram of the testing setup. (C) Photograph of the LED connected to a fluorescein isothiocyanate filter set (FITC) cube and extension tube. (D) Photograph of dPCR chip placed on a silicon wafer [41].

2.1.1 Design and fabrication of microfluidic silicon chip for dPCR

The silicon (9 × 9) mm² dPCR chip was fabricated. The core of the dPCR chip forms six blocks, each containing a defined number of wells. Additionally, it also contains cross alignment marks to simplify the dPCR image processing. The microwells have a different diameter from 50 μ m down to 5 μ m, and the total number of wells is from 26 448 to 1 656 000 (Table 2). The experiments presented here utilized the chips with 26 448 wells with a target diameter of 50 μ m and a target depth of 30 μ m. The chips with different well diameters were not tested due to their parameters below the camera's resolution. The optical system has to be improved to increase its resolution, and next, the chips with different well diameters can be tested.

Table 2 Parameters of four different dPCR chips. Reproduces from [42].

Well diameter [µm]	Total number of wells	Number of wells in one segment	Total volume [μL]	The volume of a single well [pL]
50	26 448	4 408	1.56	59
20	139 896	23 316	0.84	6
10	475 272	79 212	0.37	0.78
5	1 656 000	276 000	0.17	0.1

A representative commercial product of cdPCR is the QuantStudio 3D chip, having 20 000 ≈60 µm hexagonal microreaction chambers etched into the silicon chip [43]. The silicon-based dPCR chip is convenient for batch processing and system automation. The price of one chip for QuantStudio 3D is

≈278 Kč; compared with the price of our fabricated chip after introduction into mass production, the price would be lower 10×, approximately ≈20 Kč/chip and on the top of that, these silicon chips are reusable making the dPCR experiment much cheaper.

The detailed microwell design of the dPCR chip is shown in Figure 6 - 7. Figure 6 shows the small portion of the round microwells. The photograph of the central part of the chip represents the area of the chip divided into four separated blocks. The photograph of the lower right corner represents the area of the chip with cross alignment mark to simplify the dPCR image processing, the microscale to check the microfabrication process, and the acceptable range of well diameters. The inset images were captured by microscope (Zeiss, Axio Imager.M2m) at a magnification of 5× and 10×, respectively. The entire dPCR chip was a photograph from a camera, part of the dPCR platform.

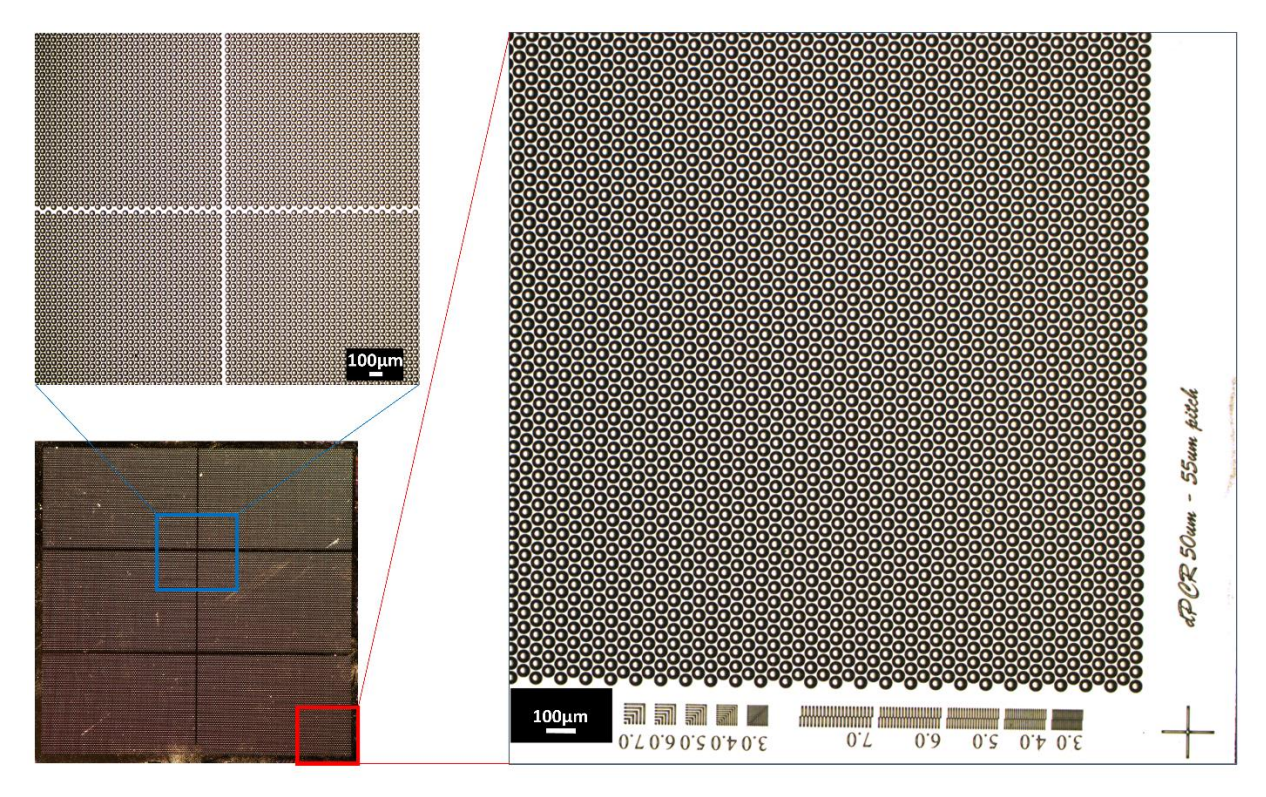


Figure 6 The photograph of the entire dPCR chip with a designed diameter of a microwell ≈50 µm showing details of the central part of the chip (blue inset) and lower right corner with the cross alignment mark on the edge of the chip (red inset).

The photographs of the dPCR chip and its cross section from the scanning electron microscope (SEM) (Tescan Lyra3) are shown in Figure 7. The actual parameters of the microwells were slightly different from the design, resulting in microwells with a diameter of ≈51.3 µm (Figure 7A) and a depth ≈24.94 µm (Figure 7B). The deviations were caused during the fabrication process of microwells. Moreover, the DRIE method of microwell fabrication is a cyclic process that forms small scallops at the inner walls of the etched structures. These defects of DRIE etching are visible in the images (Figure 7A, B) and can influence the target amplification resulting in the defects during thermal cycling [44]. Two more SEM images captured the different views of microwells cross section (Figure 7C) and microwell depth (Figure 7D).

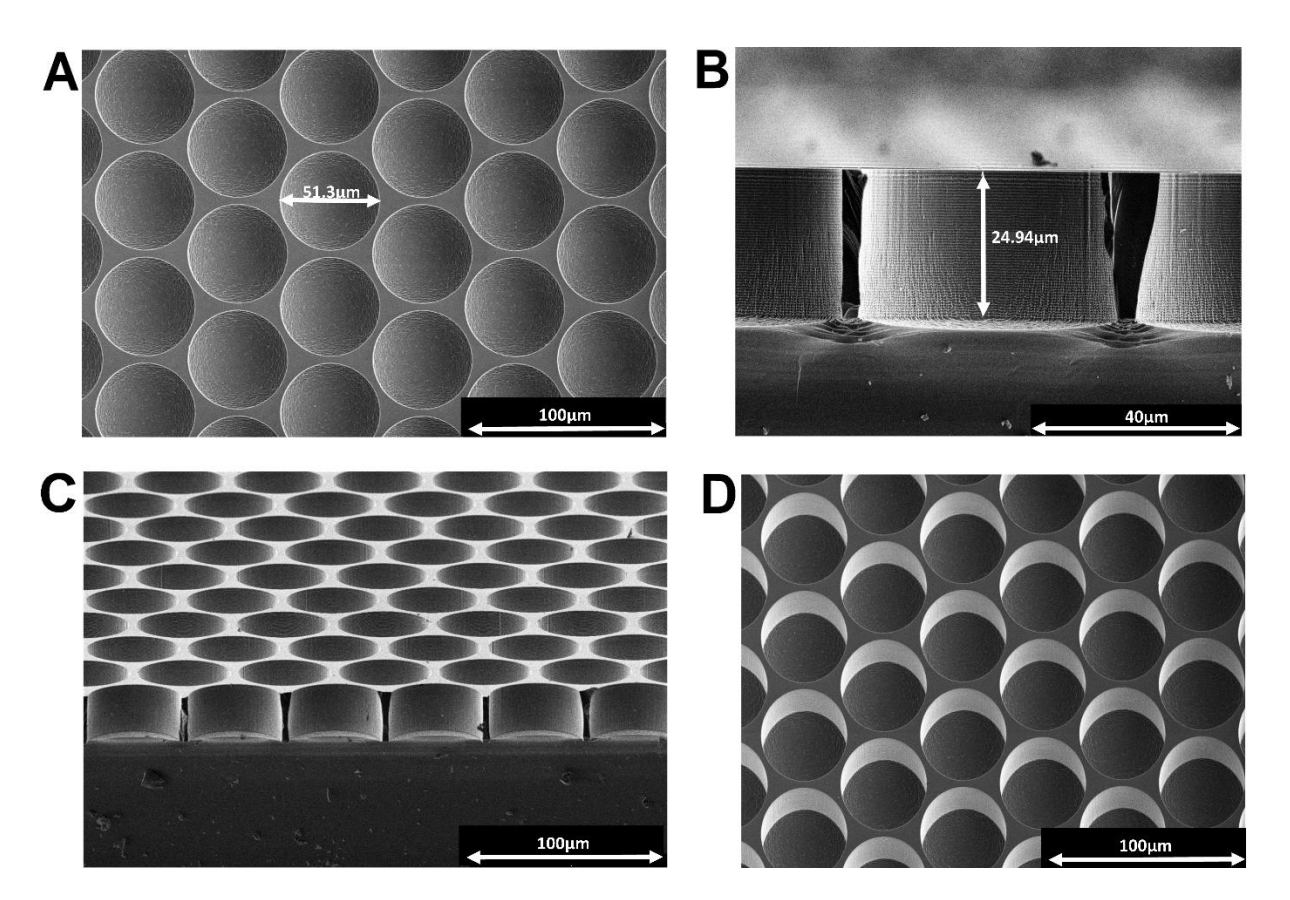


Figure 7 Images from SEM showing a chip of microwells with (A) designed diameter of ≈50 μm and (B) targeted depth of ≈30 μm. (C-D) Different views of a small portion of microwells.

2.1.2 Parylene C deposition protocol of cover glass for dPCR

The loaded chip with the sample was covered with a glass microscope coverslip ≈(10 × 10) mm² in size and coated with PDMS and Parylene C to suppress PCR master mix evaporation and limit well-to-well cross-contamination during the thermal cycling [42]. The chip packaging structure was insufficient, and the sample was evaporated at high temperatures. Thus, the hydrophobic and soft nature of the glass coverslip coated with Parylene C over the PDMS layer was enhanced by pipetting the mineral oil layer to prevent the solution from one well contaminating the solution in the neighboring wells and its evaporation. The utilization of mineral oil for cdPCR is well known. The PCR-grade oil has to be deposited onto the loaded chip of QuantStudio 3D [38]. The experimental silicon microwell-based dPCR chips were sealed by mineral oil [45].

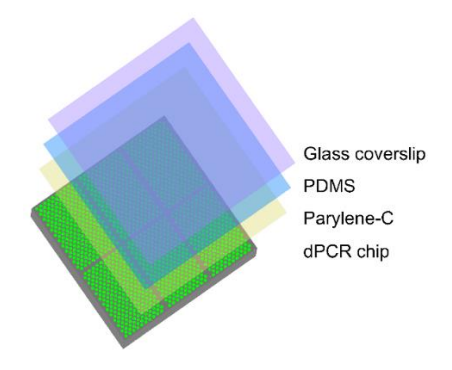


Figure 8 Schematic of the layered chip packaging structure. The non-volatile cover is formed by the bonding of glass and the PDMS and then coated with a layer of Parylene C. Reproduced and modified [42].

2.1.3 cdPCR applications and multiplexing

PCR has become one of the most widely used techniques in molecular biology. The fundamentals of the method are the same for all evolution variants of PCR. They differ mainly in the detection of amplification products and the method of sample loading. dPCR is the end-point detection method. Here is presented a dPCR platform using the same PCR chemistry for the master mix as for the droplet qPCR. The developed platform employed a single fluorescent channel and intercalating dye EvaGreen to determine the PCR product specificity based on MCA. The same method is applied for duplex detection of two target genes, chromosome 21 (Chr21), and chromosome (Chr18).

2.1.3.1 The microwell chip sample loading optimization

After microwell chip and cover glass fabrication, the next step was to find a suitable sampling method to improve the loading efficiency, thus ensuring precise amplification. The dPCR chip was loaded with a master mix covered with the glass, and thermal cycling was performed to test the amplification. The images of the amplified chip at the end of the dPCR contained defects due to sampling. Incorrect sample loading method gave rise to the defects, and the quantification of amplified area of dPCR chip was useless. The various methods were tested. The most common flaws during dPCR are shown in Figure 9. The dPCR chip without amplified area (Figure 9A, C) results from increased pressure and clamp application during thermal cycling, respectively. Evaporation of the sample (Figure 9B, C) was caused by a wrong manipulation with the chip. It is important not to touch and not move the cover glass after sampling. As soon as the glass was only pressed by tweezer to make the seal between the chip and the glass stronger or with the clamp, it resulted in sample evaporation. The damage by cluster formation was caused by an excess of a sample on the chip (Figure 9B) or by bubbles formation (Figure 9D). The sample volume was optimized for 4 µL, and the second unfilled dPCR chip was placed behind the tested chip during the sample spreading to drain the sample in excess. The bubbles were created at high temperatures of denaturation steps. The reason could be the scallops at the microwells' inner wall, which can act as nucleation sites for bubbles [44]. Thus the quality of fabricated dPCR chips influenced the amplification results. The problems with the bubbles generated at high temperatures in PCR oil were also mentioned for the commercial dPCR chips [38].

The final sample loading protocol was as follows, dPCR chip was treated in O_2 plasma, the volume \approx 4 µL of sample master mix was pipetted on the edge of the dPCR chip, and the sample was then spread by the glass, the excess of the sample was drained into the second chip. Then \approx 10 µL of mineral oil was pipetted on the edge of the cover glass, coated with Parylene C and PDMS, and placed on top of the dPCR chip to cover the sample in the micro partitions. Optimized protocol improved the amplification results, and the images were processed by MATLAB to quantify them.

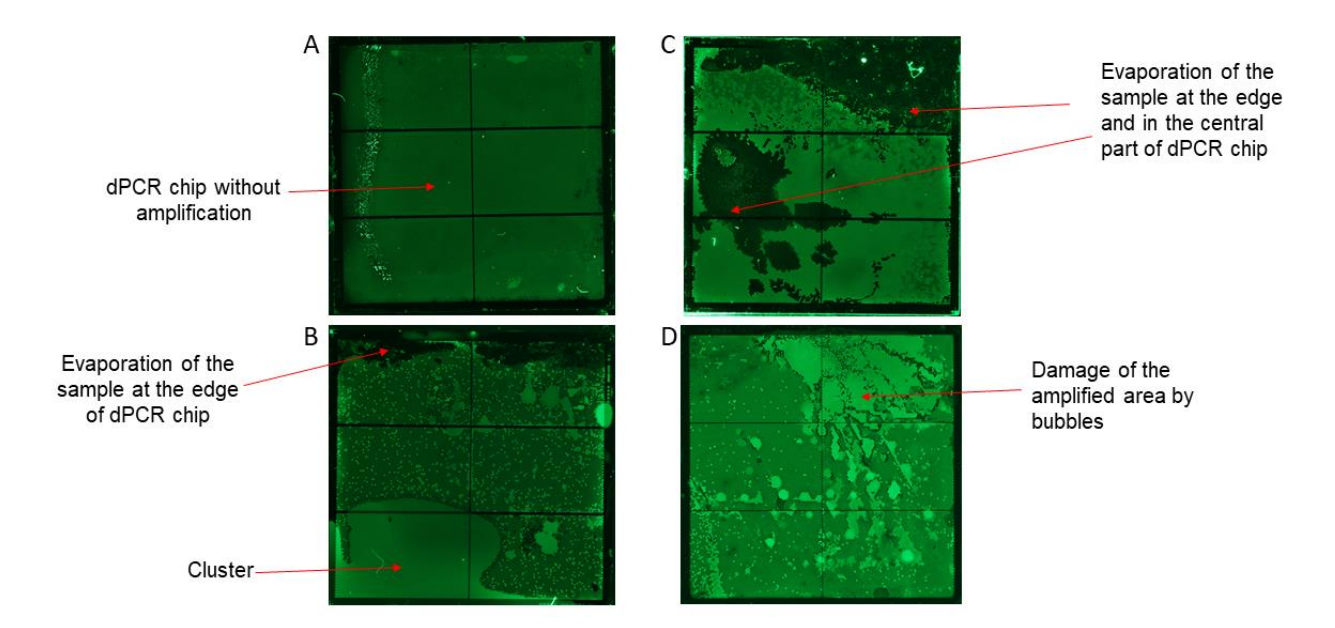


Figure 9 Results of incorrect sample loading resulting in amplification defects. (A) dPCR chip with the sample at the end of PCR without amplification. (B) An amplified area on chip damaged with cluster (created from a master mix in excess) and evaporation. (C) dPCR chip with the sample at the end of PCR without amplification and damaged with evaporation. This chip was pressed with a clamp during the thermal cycling. (D) An amplified area on the chip was damaged with the clusters created from bubbles.

2.1.3.2 Temperature non-uniformity detection on dPCR chips (published in [41])

The following section 2.1.3.2 is reproduced from publication [41]. Temperature uniformity between partitions is critical as the temperature during thermal cycling affects PCR efficiency [46]. The thermal uniformity of the dPCR device depends on its heating/cooling elements and the thermal conductance between the elements [47]. The most commonly used heating/cooling techniques are based on TEC [48]. Other techniques, based on different principles, can also be used, such as photonic heating with airflow cooling [49]. Additional problems arise from non-uniform temperature distribution due to insufficient heat transfer or non-uniform cooling in open systems such as air convection [50]. This is a significant problem as the relative PCR efficiency between partitions is strongly affected by poor temperature uniformity during thermal cycling [51]. Therefore, each dPCR assay must be optimized carefully, and the reasons causing false positive signals are more easily detectable than the causes of false negative partitions. Attempts to prevent false negative dropouts mainly focus on optimizing the surface to volume ratio of partitions, which potentially inhibit the PCR process, or on pre-analytical steps associated with preparing the DNA template [52]. When optimizing dPCR on a chip, thermal nonuniformity is usually not considered as a measurement of sample temperature (Ts) inside partitions with a sample volume of pico-/nano-liters is a challenging job [53, 54]. An accurate system to calibrate a temperature sensor with respect to the fluid inside the partitions and enable determination of the temperature distribution over the dPCR chip, or even between the partitions, would benefit the optimization of temperature uniformity [55], thus improving PCR efficiency.

The method presented the way of non-contact localized temperature measurement for the determination of the non-uniformity of temperature distribution over a dPCR chip. Among the non-contact temperature measurement methods, the proposed $T_{\rm M}$ based method can determine the temperature distribution into the chip instead of only the chip surface. Besides, it removed the negative

photobleaching effect of the fluorescein-based temperature measurement method. Temperature determination over the dPCR chip, based on $T_{\rm M}$, allowed calibrating the temperature sensor and improving the dPCR configuration and precision. The method described here thereby characterized the distribution of temperature non-uniformity using a PCR solution with known $T_{\rm M}$ as a temperature sensor. This method is also suitable for determining the temperature uniformity of other microarray systems where there is no physical access to the system. Thus direct temperature measurement is not possible.

The entire data acquisition process (Figure 10A, B) started with qPCR sample preparation by mixing the PCR master mix with the synthetic HBV template, amplification, and performing MCA to determine $T_{\rm M}$ (Figure 10C, red curves) the sample using a commercial thermal cycler. Then the dPCR chip was filled with the amplicons covered with mineral oil and cover glass was placed under the dPCR configuration to perform MCA. The F images of the dPCR chip were captured at different values of $T_{\rm S}$, starting at 25°C and then in the range from 70°C to 94°C (Figure 11). A MATLAB-based script was used to process the F signal after taking a series of images at various temperatures below and above $T_{\rm M}$.

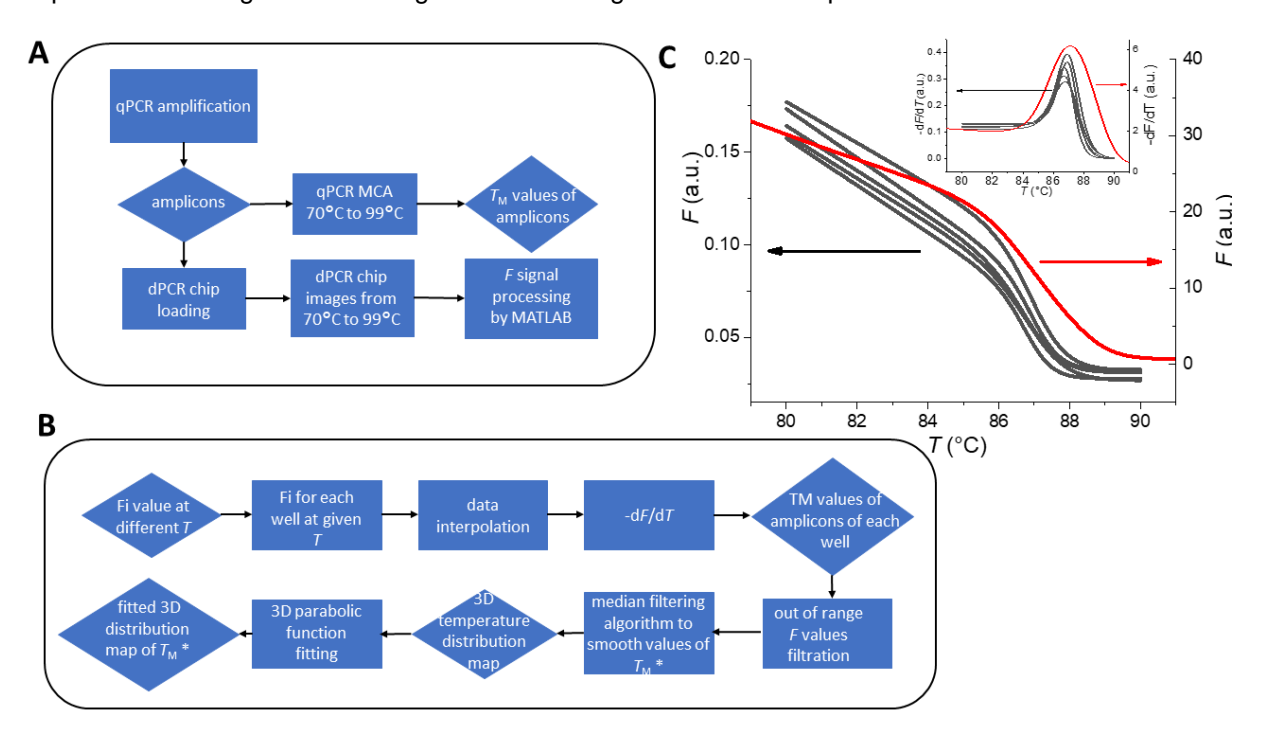


Figure 10 (A) Schematic diagram of data acquisition. The diamonds represent the output results of measurement or data processing, and the rectangles represent the measurement method or data processing method. (B) Block diagram showing the data processing with MATLAB script used to obtain the distribution of melting temperature of dPCR chip partitions ($T_{\rm M}^*$). The scrip evaluated simultaneous MCA at each partition over the whole dPCR chip. (C) MCA from qPCR (red) and MCAs from dPCR (black) and their -dF/dT values (inset), again with qPCR data in red. Reproduced from [41]

First average fluorescent intensity (F) values were extracted of each partition at given T from all images and were saved into a file set. Subsequently, a piecewise cubic interpolation was performed at an interval set to 0.01°C on the file set and obtained the F values of each partition as a function of assumed T, extracting MCAs from all partitions of the chip. Then was performed the -dF/dT and the measured values of T_M * were acquired. Due to defects such as empty partitions, flaws in the cover glass, or chip damage, some T_M * values deviated from the mean value by more than 1°C. These out-of-range T_M * values were not considered in calculations. A few melting curves from partitions for HBV target are shown in Figure 10C, black curves.

Subsequently, we built a discrete two-dimensional (2D) (Figure 12A) and three-dimensional (3D) (Figure 12B) $T_{\rm M}^*$ distribution map as a function of partition positions, followed by a median filtering algorithm to smooth the maps. Then we performed parabolic function fitting on the 2D and 3D map and constructed the fitted $T_{\rm M}^*$ distribution maps (Figure 12C, D) of the dPCR chip. The fitted 2D and 3D map with continuity showed a trend in dPCR chip temperature distribution more clearly than the original data, with a distinguishable temperature gradient across the dPCR chip.

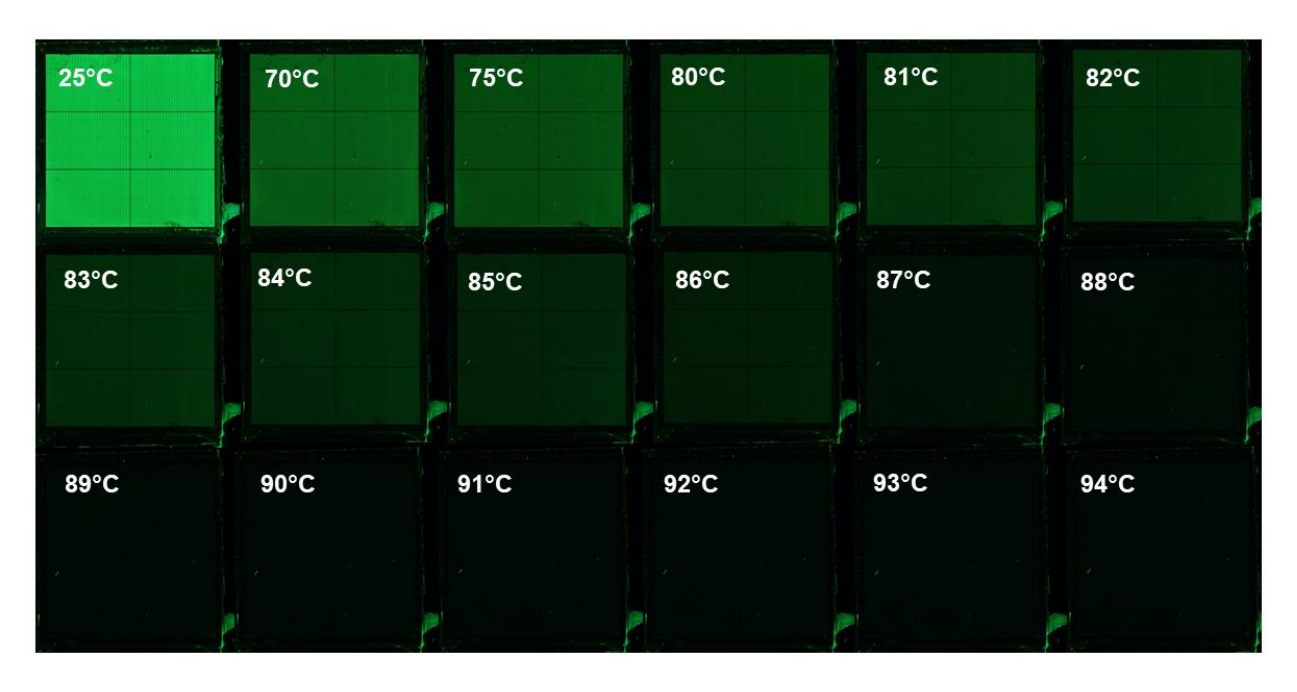


Figure 11 Eighteen fluorescent images of the dPCR chip, at different *T*, showing the measurement of MCA. The chip was loaded with the PCR amplicons and covered with mineral oil and a cover glass. Reproduced from [41]

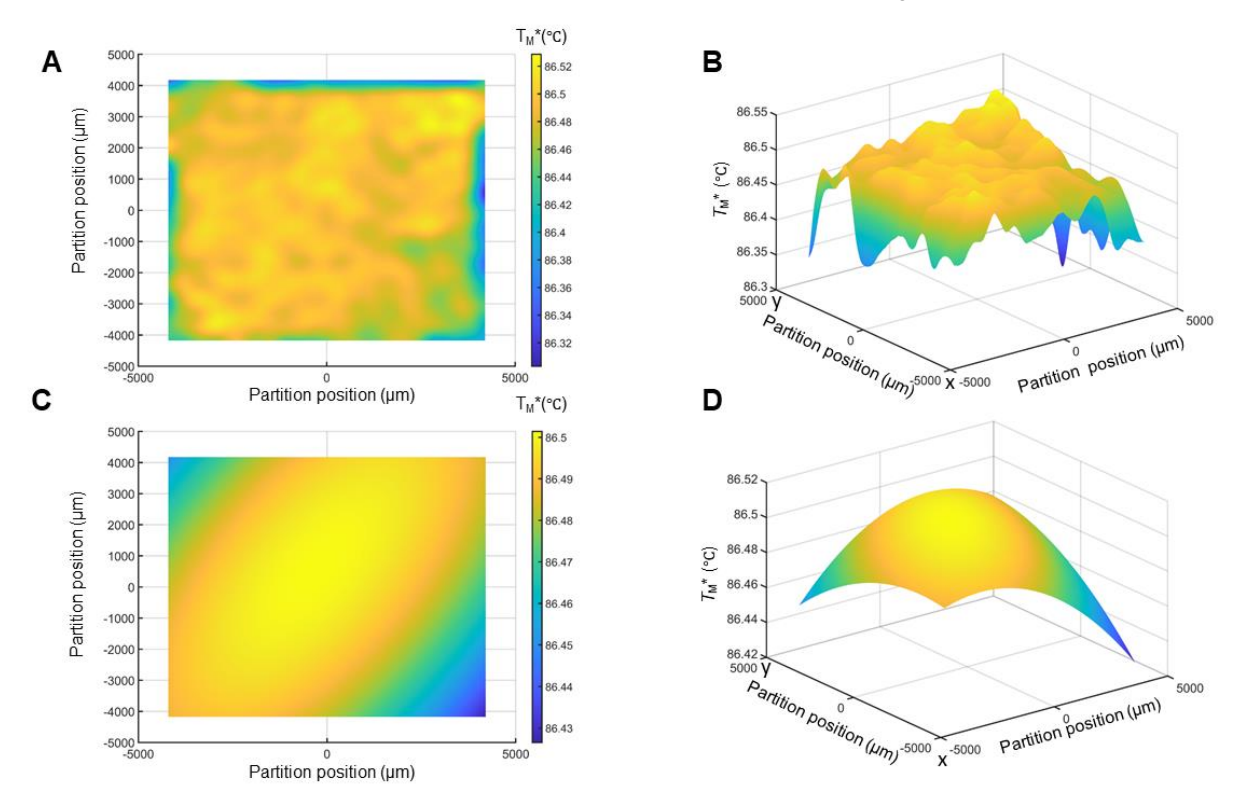


Figure 12 Temperature distribution maps of T_{M}^* . (A) Original 2D and (B) 3D map and (C) parabolic fitted 2D and (D) 3D map of HBV target gene. Reproduced and modified from [41].

The mean $T_{\rm M}^*$ value and deviation were estimated from the $T_{\rm M}^*$ values through fitting to a Gauss distribution function. The dPCR configuration yielded $T_{\rm M}^*$ equal to $(86.49 \pm 0.08)^{\circ}$ C, and the difference between $T_{\rm M}$ and $T_{\rm M}^*$ was only ≈ 0.68 °C (Figure 12A, C). This shows a good temperature homogeneity across the dPCR chip extending over the whole configuration, including the Pt100 temperature sensor. An equivalent 3D temperature map of the chip was created (Figure 12B, D). The configuration, with a (30 × 30) mm2 TEC and a piece of Si wafer as an interface between the TEC and the dPCR chip, has a superior performance with the temperature difference between the cold and hot parts of the dPCR chip only ≈0.22°C. These data demonstrated efficient heat transfer between the TEC and the dPCR chip with the Si interface. The prevention of temperature non-uniformity on a dPCR chip is critical during assay optimization. It can contribute to the elimination of false negative partitions and the removal of the socalled rain caused by inaccurate annealing temperature in the rain-forming partitions. The presence of this artifact makes it very difficult to interpret the results as it complicates the correct setting of the fluorescence threshold between positive and negative partitions [56]. Moreover, the proposed method is not affected by the heat capacitance of the temperature probe or the small sample size as with traditional temperature sensors. Knowing that there is a problem with either the temperature or its inhomogeneity gives engineers a guide to redesign the system to correct these values and thus improve dPCR accuracy. All temperature data are summarized in Table 3.

Table 3 Results of $T_{\rm M.}$ Reproduced from [41].

Target	Room T	Sensor T	T _M by qPCR	T _M * by dPCR	$ T_{M}^* - T_{M} $	Min T _M * by dPCR	Max T _M * by dPCR
gene	[°C]	[°C]	[°C]	[°C]	[°C]	[°C]	[°C]
HBV	19.0	14.6	87.17 ± 0.04	86.49 ± 0.08	0.68	86.30	86.52

The difference in T_{M}^* and T_{M} values shows the importance of sensor calibration. This was also demonstrated earlier when the readout of the resistive temperature detector (RTD) sensor calibrated traditionally differed from the actual fluid T by almost 10°C [57]. We used T_{M}^* relative to T_{M} as the first calibration point. The second calibration point was obtained by comparing the integrated Pt100 sensor value with an external thermometer. The configuration being measured having the power for the TEC off, thus assuring the temperature of the dPCR chip had equalized with the ambient environment (Figure 13).

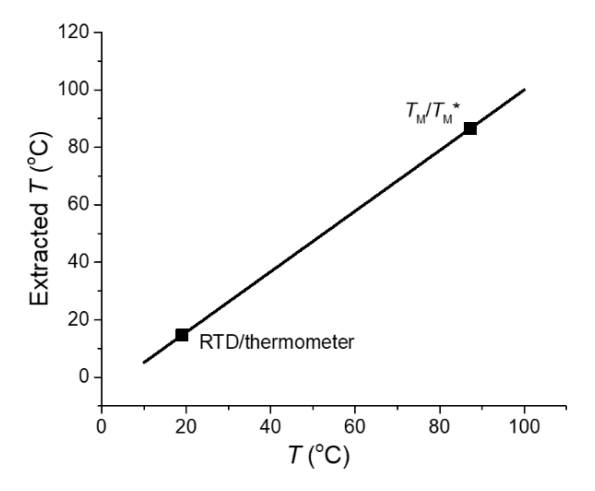


Figure 13 Two-point calibration of the temperature sensor. Reproduced from [41].

A similar fluorescence measurement technique, based on MCA of DNA, has been utilized early [58]. The $T_{\rm M}$ depends only on the composition of the DNA template and the PCR master mix, making it independent of photobleaching. The F value decreases with exposure time; however, the first derivation of the melting curves with respect to $T_{\rm S}$ provides the constant value of $T_{\rm M}$ with minimal deviation [58]. This MCA-based non-contact temperature measurement technique was previously applied to determine the temperature uniformity inside the microfluidic channel of a microcalorimeter. The device was subsequently calibrated accordingly [57, 59].

There are alternative methods to measure T_S utilizing contact or non-contact methods. Contact methods primarily use temperature sensors [16, 49, 60] such as RTD [61], thermistors [16], or thermocouples [62] for point measurement. However, it is impossible to determine T_S within a single micro/nano partition using those sensors due to the size limitations [57, 63]. The most popular noncontact temperature measurement method is based on an emitted infrared (IR) power determination [16, 49]. This only determines the power of the IR radiation emitted from the surface, which for these chips is typically that of a glass covering the partitions inside the chip, meant to prevent water evaporation from the PCR master mix [42]. Unfortunately, the glass is not transparent at IR wavelengths, making it impossible to determine the T of the master mix, which is the most critical information for optimal PCR operation. The measurement precision can also be affected by surface contamination. Other non-contact temperature measurement methods use the fluid in the partitions as a sensing element, via the inclusion of thermochromic dyes, such as organic leuco dyes, with specific temperaturedependent optical properties [64]. However, these methods are restricted to temperatures up to ≈50°C, insufficient for dPCR applications. An obvious alternative would seem to be fluorescein, as its amplitude of F is a function of T [65], and fluorescence measurements are compatible with the instrumentation used for dPCR quantification. Unfortunately, this technique is susceptible to photobleaching, and thus the system cannot be calibrated for precise temperature determination.

2.1.3.3 Single gene dPCR amplification

The PCR master mix of synthetic HBV gene was prepared and initially verified using a commercial PCR cycler to identify $T_{\rm M}$ of amplicons; $T_{\rm M}$ for HBV was $\approx 87.2^{\circ}$ C (data not shown). The same PCR protocol was then performed in a dPCR chip on the TEC, and the F images of the dPCR chip were captured at each thermal cycle (Figure 14) at the end of the elongation step. The detail of positive wells (PW) and negative wells (NW) is shown in Figure 15. The MCA was captured at the end of thermal cycling, ranging from 70°C to 95°C (Figure 16).

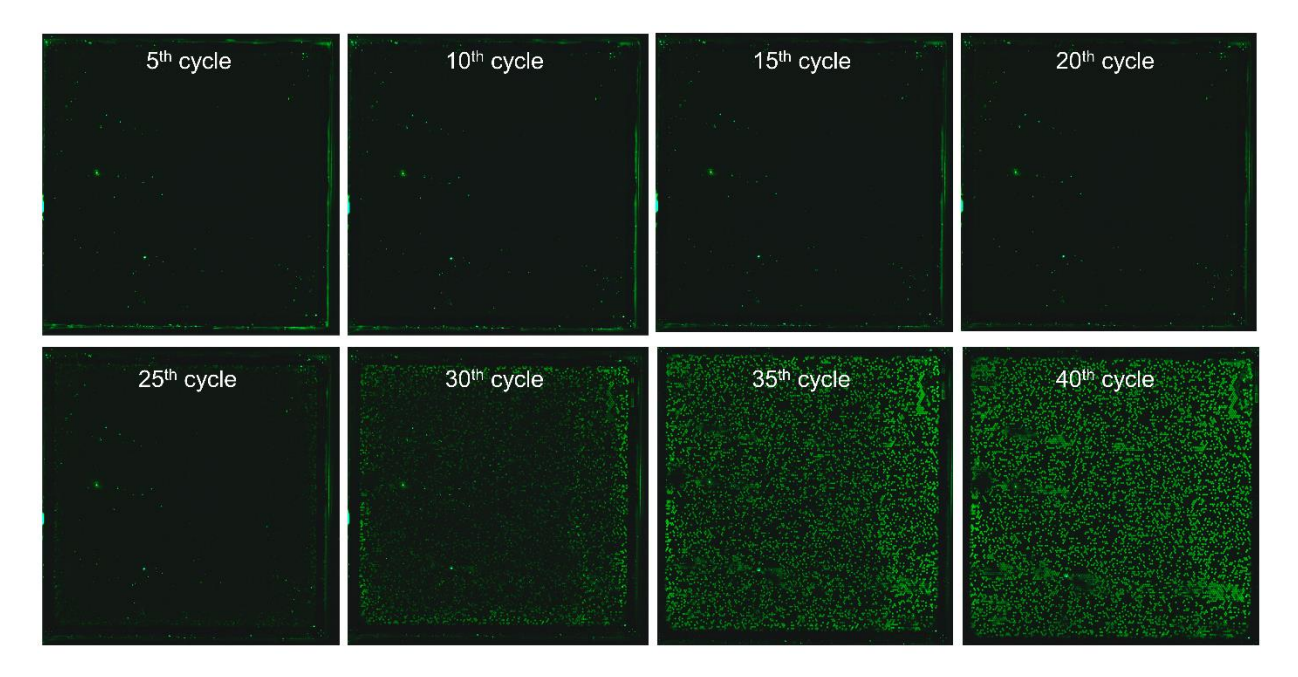


Figure 14 Fluorescent photographs of dPCR amplification progress captured at the end of elongation step showing each fifth thermal cycle.

The dPCR chip was loaded using a solution with copy number (cn) of 11 232, corresponding to the average copy number in each partition (λ) value of 0.42 copies partition 1. The F signal exceeded the baseline, and the target HBV gene started to be amplified between the 25th and 30th cycles. The 40th cycle was the last one, and the F signal reached its plateau phase. The area of an amplified chip (Figure 15) with its PW and NW contain the contaminants (defects) with the higher F_i . The contaminants could result from the fabrication defects of the chip or the glass or contaminants in the master mix (dust, precipitated particles). Measuring the MCA, the F of contaminants does not change, and the recognition of amplified wells and contaminants is clear. The F_I of PW wells was slightly different. Some of the wells could contain two or more DNA copies, having the higher F [66]. Therefore, the results are processed statistically. Poisson statistic is used to evaluate the dPCR experiment. Some of the wells could be amplified with lower PCR efficiency; however, the experiments proved homogeneous temperature distribution at the dPCR chip. Thus, some of the wells could be more likely influenced by the neighboring wells, for example, the well to well cross contamination. The well-designed, optimized assays are also crucial for absolute quantification and the specificity of the reaction [67, 68]. Primers must be designed specifically for a particular DNA segment to avoid highly homologous sequences and ensure even amplification of all targeted DNA fragments. Poor design or optimization may lead to overestimation due to nonspecific amplification, which means positive signals in the absence of a target sequence [67, 69]. These false positives reduce specificity. On the other hand, inhibitors or non-optimized time and temperature programs may fail to reach the fluorescence threshold while still containing at least one initial target copy [69].

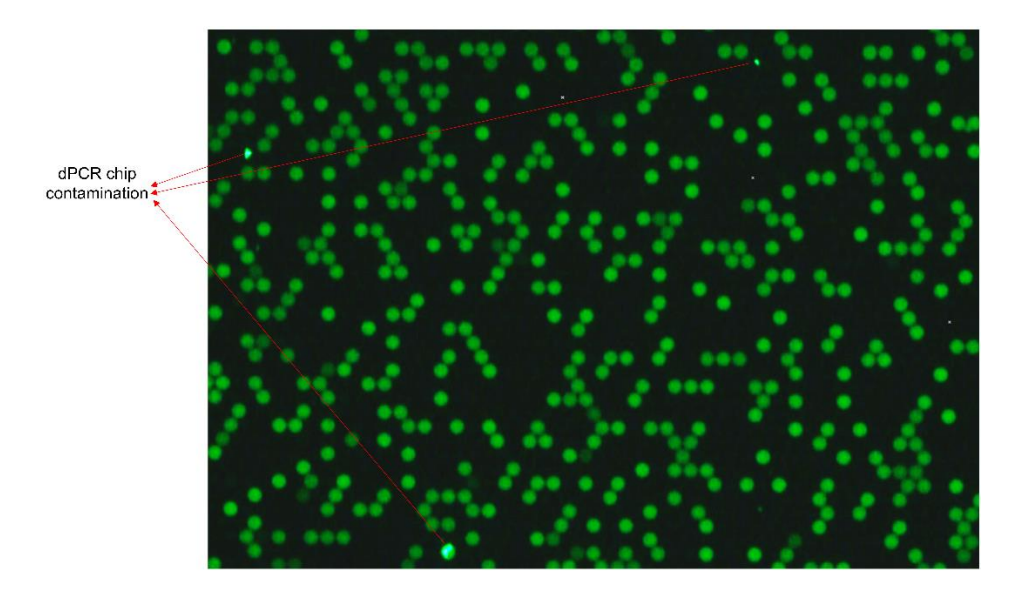


Figure 15 The detail of dPCR chip amplified area with PW and NW with contaminants on dPCR chip.

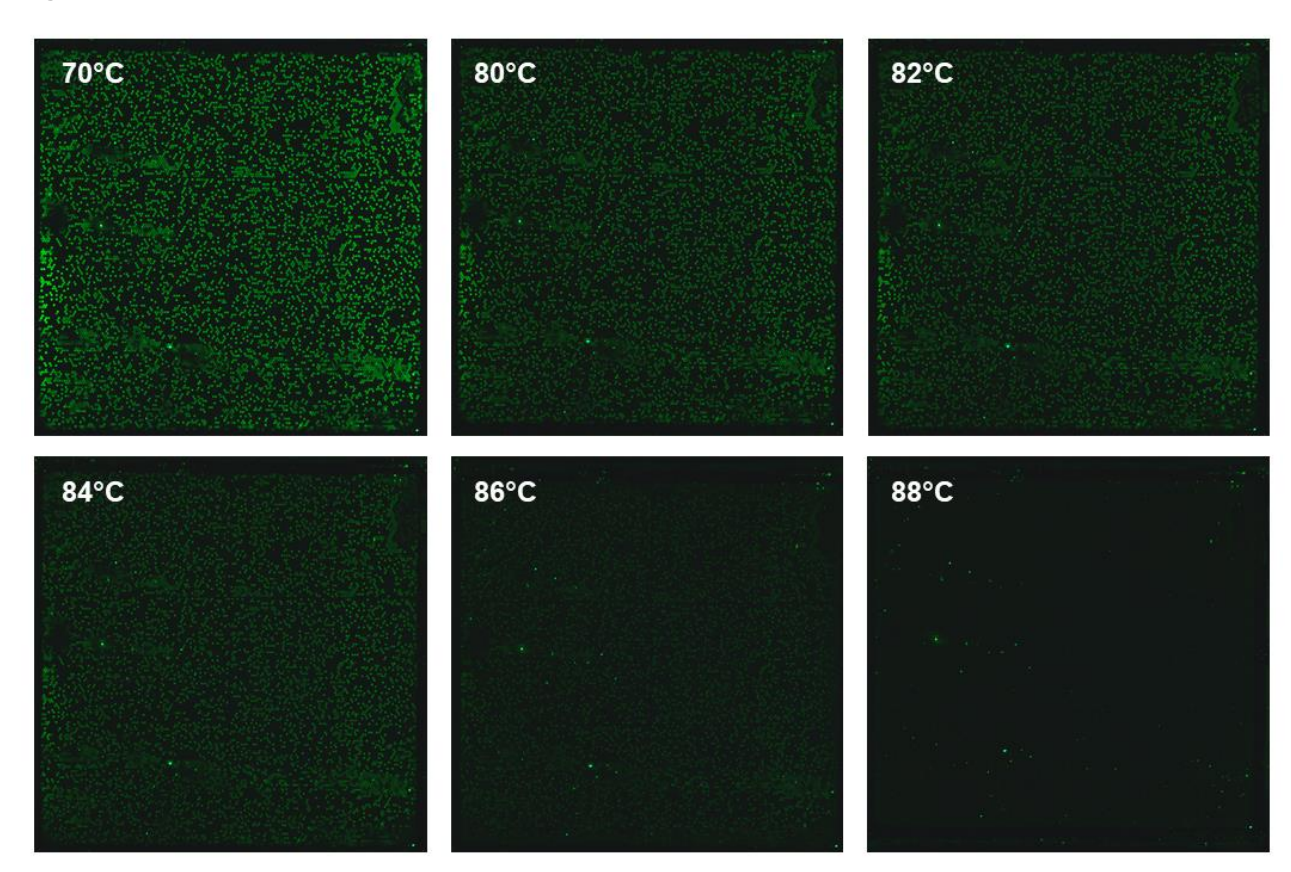


Figure 16 The MCA of amplified dPCR chip after 40 cycles of thermal cycling.

The MCA results were processed by MATLAB-based script. A MATLAB script was used to process the F signal after taking a series of images at various temperatures (Figure 16) below and above $T_{\rm M}$. A few melting curves from four partitions for the HBV target are shown in Figure 17A and its $-{\rm d}F/{\rm d}T$ in Figure 17B. The dPCR yielded $T_{\rm M}^* \approx 86.4\,^{\circ}$ C, and the difference between qPCR $T_{\rm M}$ ($\approx 87.2\,^{\circ}$ C) and $T_{\rm M}^*$ was only $\approx 0.8\,^{\circ}$ C. The temperatures deviations between the two PCR platforms are similar to the previous experiments. The assay yielded good PCR sensitivity and efficiency. The subsequent step was dPCR amplification of the HBV target gene of various λ values.

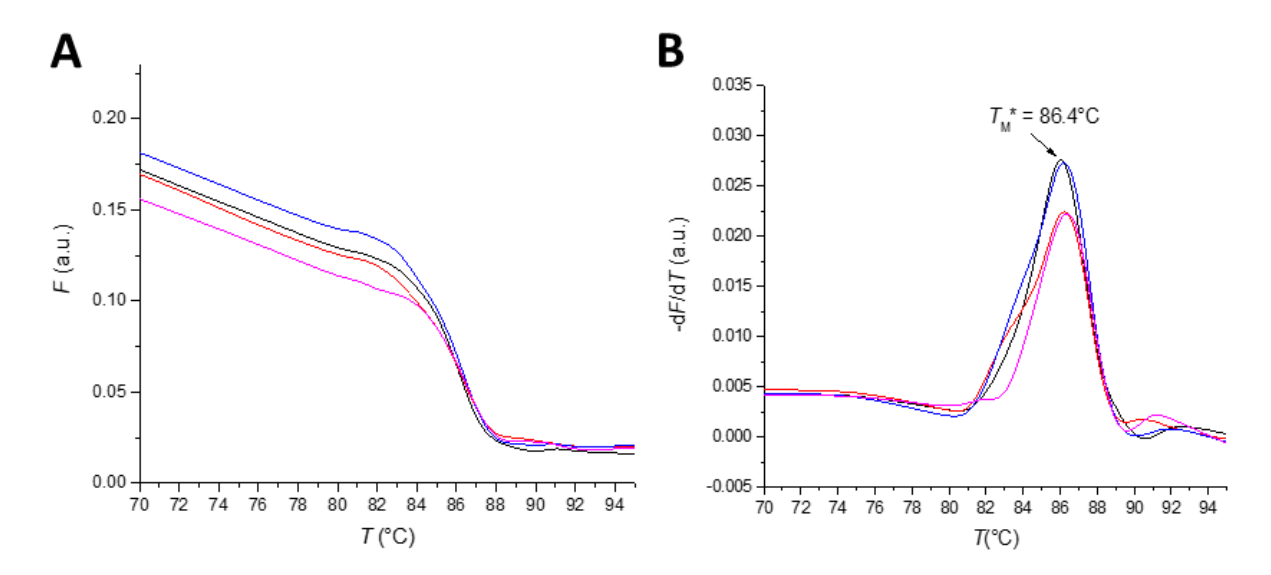


Figure 17 Melting curves from four microwells for HBV gene after dPCR and their -dF/dT values.

The following results (Figure 18 - 19 and Table 4) are reproduced [70]. The dPCR chips were loaded by a master mix solution containing synthetic HBV with a λ value in the range of 0.8 - 0.1 copies partition 1, corresponding to cn of 22 464 – 2 808. Then, temperature cycling was performed using the above protocol. Once the PCR was completed, a fluorescence image at 25°C was acquired. Here, is showed dPCR amplification of the chip's image before light-nonuniformity correction (Figure 18). Subsequently, the F values were extracted from each partition using the proposed algorithm. The histogram (Figure 19) of occurrence as a function of F value was built for different HBV dilutions. The number of PW and NW (Table 4) was determined based on the histogram, and a derived Poisson distribution was used to obtain the λ values to validate the experiments. The values difference between the input λ and calculated λ was due to the imperfect sample loading to the chip and defects caused during the amplification process, such as some evaporation or bubbles formation during thermal cycling.

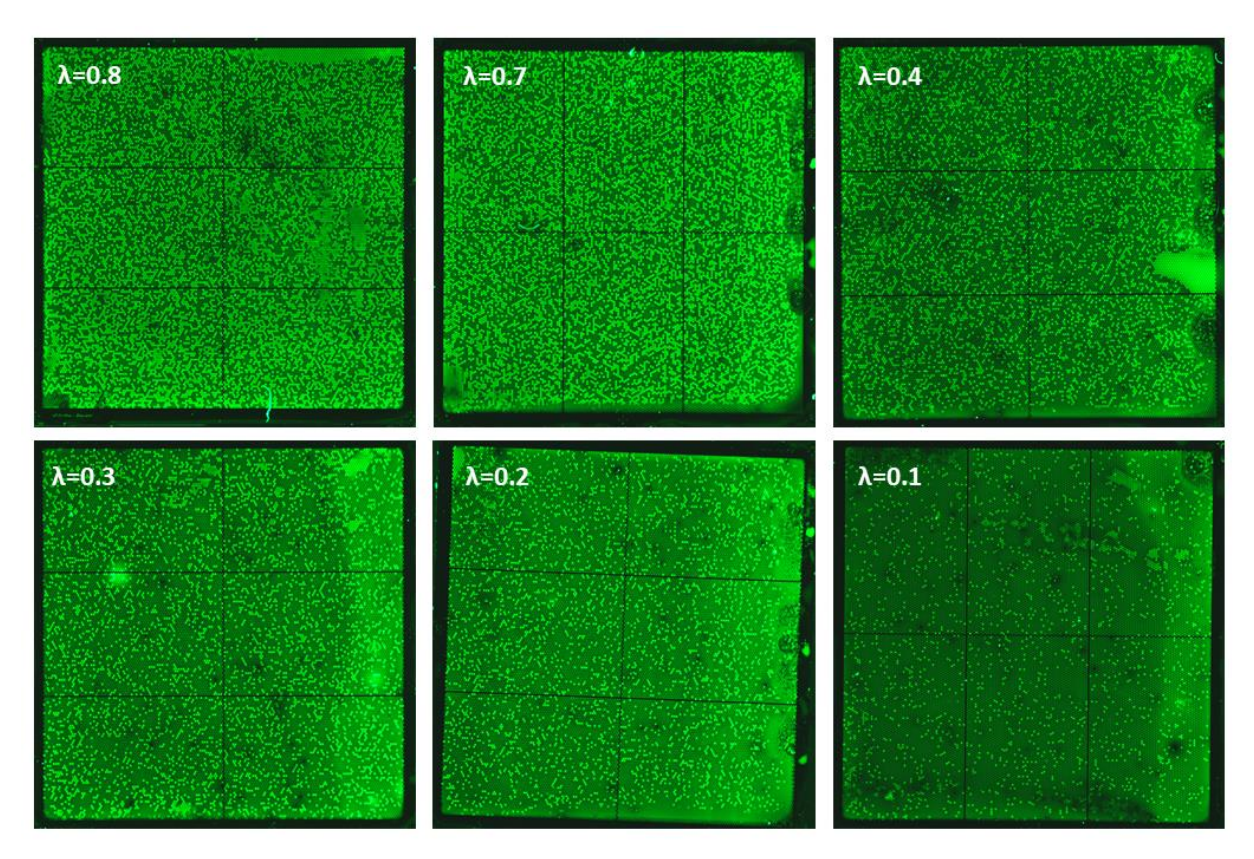


Figure 18 A photographs of amplified dPCR chip with different λ values of synthetic HBV target gene at 25°C. Reproduced from [70].

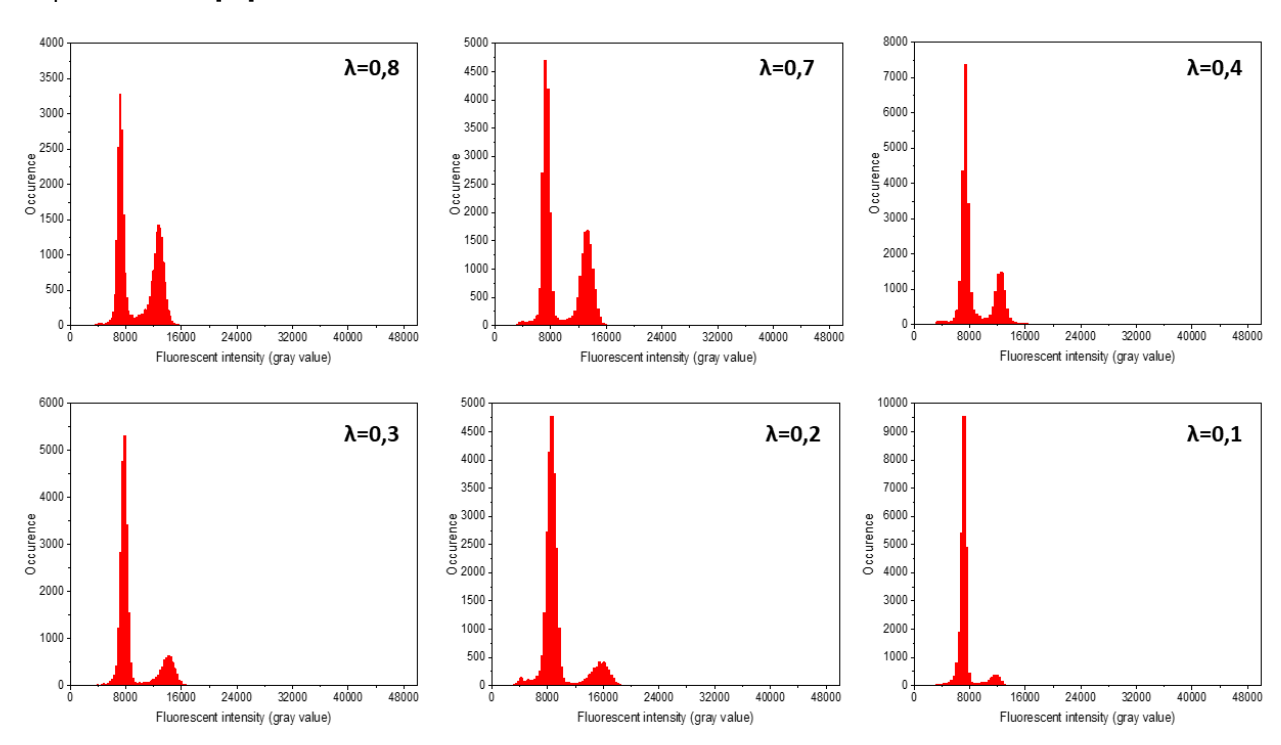


Figure 19 Extracted histograms of occurrence as a function of fluorescent intensity for different λ values of synthetic HBV gene. Reproduced from [70].

The partitions with higher F values were PW, and those with lower F values were identified as NW. The number of amplified wells is decreased with the decreasing λ as well, as the histogram peaks of PW are decreased.

Table 4 Processed results of amplified dPCR chip with different λ values of synthetic HBV target gene. Reproduced from [70].

Input DNA cn			Calculate DNA cn				
cn	λ [copies·partition ⁻¹]	PW	NW	PW	number of wells	λ [copies·partition ⁻¹]	cn
22 464	0.85	15 137	14 433	12 004	26 437	0.61	16 008
18 720	0.71	13 416	15 634	10 784	26 418	0.52	13 875
11 232	0.42	9 152	19 526	6 908	26 434	0.30	8 011
8 022	0.30	6 920	21 062	5 369	26 431	0.23	6 005
5 616	0.21	5 060	22 608	3 833	26 441	0.16	4 142
2 808	0.11	2 664	23 725	2 691	26 416	0.11	2 842

The experimental results showed that our algorithm obtained quantitative data corresponding to the expected values. However, the imperfect loading of the sample to the chip and some evaporation during thermal cycling led to a significant error between the input and calculated λ values, primarily due to concentrated sample filling of the chip [42]. However, the input and calculation results of the most dilute sample (with λ = 0.11 copies-partition⁻¹) are similar with a small deviation. The imperfect loading and the heating appeared even with the amplification using commercial dPCR chips. The discrepancies in the number of loaded partitions and the number of amplified partitions with commercial QuantStudio 3D digital PCR chip were published [71].

The proposed algorithm is designed independently of dPCR chip structure damage and light intensity non-uniformity. Therefore, it also provides a reliable alternative when analyzing the results of chip-based dPCR systems. Furthermore, compared with a conventional image processing algorithm, this algorithm is designed to process dPCR images with known defects, such as a damaged chip structure, incomplete chip filling, assembly error, and light non-uniformity. This characteristic might be beneficial for realizing a versatile dPCR platform, especially for future chip-based platforms. Additionally, the details of image processing algorithms in commercial dPCR systems are not available to users; thus, it is to elaborate on their merits or demerits. Only a few papers describe the chip-based image processing methods based on deep learning [72]. However, it requires a high requirement of computer configuration level and an extensive training dataset, making the detection complex and time-consuming. Previous research proposes a random background transfer-based image processing algorithm to simplify the training dataset significantly, as it only requires three experimental images [73]. However, it was used for augmenting images to lower the effect of uneven illumination rather than remove it.

The similar dPCR amplifications to the previous experiments were measured to test the highly diluted samples with λ values $4\cdot10^{-4}$, $4\cdot10^{-5}$, $4\cdot10^{-6}$ copies partition corresponding to an of 12.48,1.24 and 0.12 respectively. The last sample was negative control (NC) which did not contain the template DNA. The dPCR chips were loaded by master mix solution containing isolated full-length HBV genomic DNA to test the dPCR chip for the real samples. Then, temperature cycling was performed. Once the PCR was completed, a fluorescence image was acquired at 25°C. Here, is showed dPCR amplification of the chip's image before light-nonuniformity correction (Figure 20). Subsequently, the *F* values were extracted from each partition using the proposed algorithm. The number of PW and NW (Table 5) was

determined based on the histogram (data not shown), and a derived Poisson distribution was used to obtain the λ values to validate the experiments.

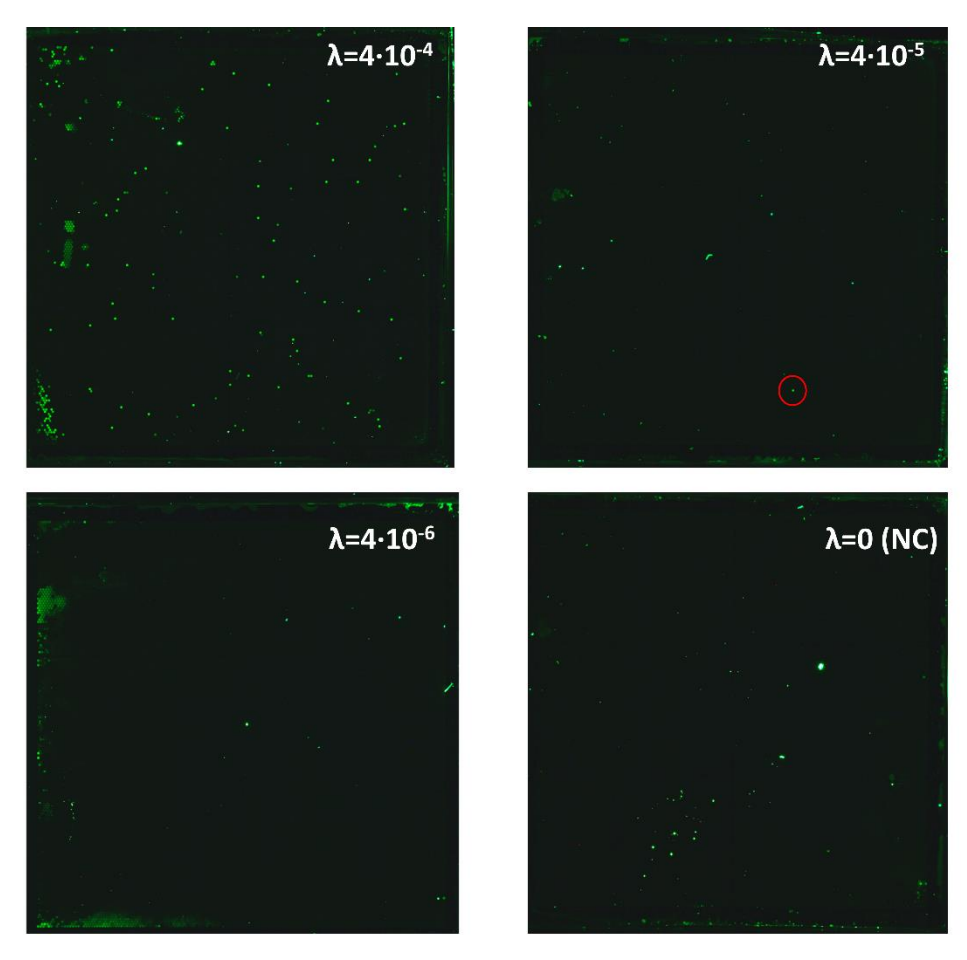


Figure 20 A photographs of amplified dPCR chip with different λ values of isolated HBV target gene at 25°C. The red circle indicated a single amplified well for $\lambda = 4 \cdot 10^{-5}$ copies partition⁻¹.

The error between the input and calculation results with the large sample dilution achieved the smallest deviation, shown in the previous experiments. Thus, the samples with the small on were tested. The isolated HBV template was amplified efficiently, such as the synthetic HBV gene. The difference between the input λ and calculated λ values here was not affected by imperfect sample loading. The defects caused during the amplification process, such as some evaporation or bubbles formation during thermal cycling as well as contaminants on the dPCR chip, occurred. Due to the small copy number of the sample, the defects did not influence the amplification. The defects could be clearly separate from the amplified wells.

Table 5 Processed results of amplified dPCR chip with different λ values of isolated HBV target gene.

Input DNA cn			Calculate DNA cn				
cn	λ [copies-partition ⁻¹]	PW	NW	PW	number of wells	λ [copies·partition ⁻¹]	cn
12.48	4.10-4	10.58	26 330	79	26 409	3·10 ⁻³	79
1.24	4·10 ⁻⁵	1.06	26 434	1	26 435	4·10 ⁻⁵	1
0.12	4·10 ⁻⁶	0.11	26 429	0	26 429	0	0

The sample with cn 12.48 yielded more PW than expected. The calculated number of PW was 79. The sample with cn 1.24 was truly amplified only in the single dPCR chip microwell, circled in red (Figure

20). After a detailed zoom, the rest of the fluorescent artefacts were only contaminants on the dPCR chip. The third sample with cn 0.12 was without amplification as well as the negative control. Quantitative data corresponding to the expected values was obtained; however, determining the limit of the detection and the sensitivity of the dPCR will require more measurements.

The sensitivity or lower limit of detection corresponds to the detection of a single molecule in a single partition. Hence, the lowest detectable concentration depends on the total sample volume or the number of partitions and their volume. The larger the total volume (due to an increase in partition size), the smaller, the lower limit of detection [52, 74]. Due to the restricted total reaction volume of various dPCR resulted in different analytical sensitivity between different platforms [6].

The amplification of the sample with the dPCR chip with different parameters is shown in Figure 21 (reproduced from [70]). The chip with partition diameters of 20 μ m was filled with a master mix of λ value 0.1 copies partition. Here the volume of the *Taq* polymerase was adjusted to 0.9 μ L due to the high surface-to-volume ratio [75]. A fluorescent image of the chip was captured and processed. The calculated λ value was 0.08 copies partition. resulting from the histograms based on extracted data. The processing details are mentioned in [70]. The image processing was challenging due to each partition's limited pixel numbers. Thus, the microwells were not well distinguished. These results could be improved by using an image with more pixels. Therefore, the rest of the dPCR chips with 10 μ m and 5 μ m were not tested for dPCR measurement.

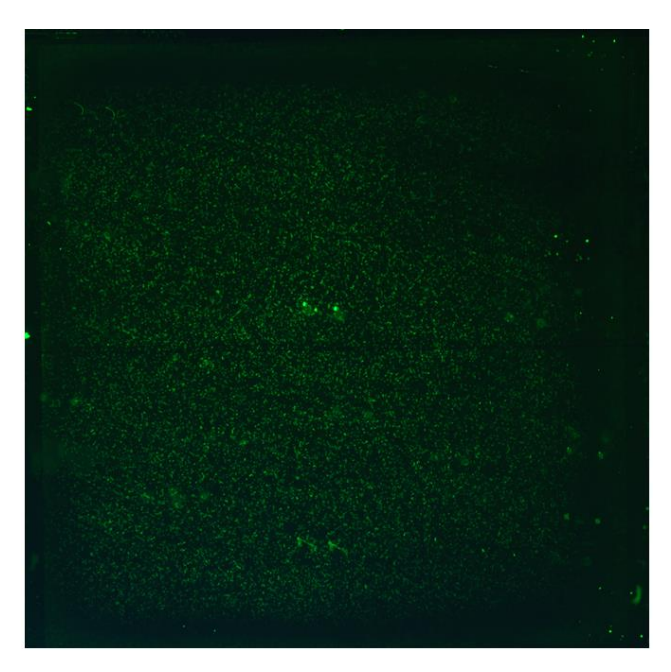


Figure 21 A fluorescence image of an amplified dPCR chip with a partition diameter of 20 μ m. Reproduced from [70].

2.1.3.4 PCR multiplexing based on a single fluorescent channel

Multiplexing is an extension of any PCR-based method. It improves the diagnostic efficiency and detection capability due to the simultaneous amplification of more genes [76], thus widely applied in molecular diagnostics [77]. Several dPCR multiplexing techniques were developed based on complex optical imaging or image processing. Here is shown dPCR duplexing method by capturing a fluorescent image of the dPCR chip at various temperatures using a single fluorescent channel. The method is

demonstrated using a combination of a sequence from Chr21 and a sequence from Chr18, both in the presence of a nonspecific intercalating dye EvaGreen.

The most common aneuploidy is trisomy of chromosome 21 (T21), which causes Down syndrome [78]. The disomy instead of monosomy of this chromosome was also detected in remarkable percentages of human ovarian cells in healthy female fetuses and in sperms of healthy men [79]. All the above mentioned results were obtained by the time-consuming techniques of fluorescent *in situ* hybridization by counting fluorescent signals in nuclei of thousands of cells. The results are of great importance for family planning in families of individuals suspected to be somatic mosaics for T21, where the dPCR could be a perspective method of prenatal diagnostics.

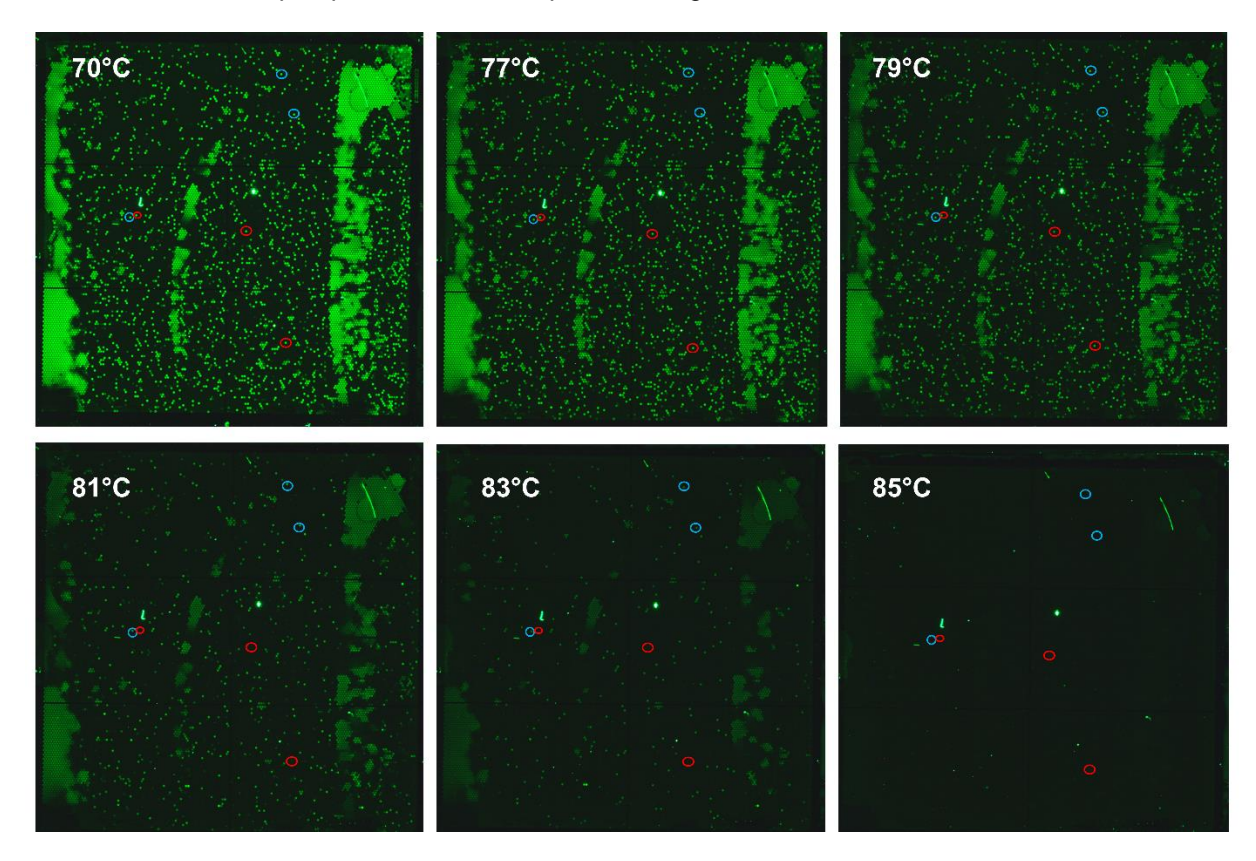


Figure 22 A photographs of amplified dPCR chip loaded with the master mix of female genomic DNA, containing target genes Chr21 (blue circles) and Chr18 (red circles) in the ratio 1:1 and its MCA.

The PCR master mix of female genomic DNA was prepared and initially verified using a commercial PCR cycler to identify $T_{\rm M}$ of amplicons. Two template sequences were contained, Chr21 and Chr18, in the ratio 1:1. The $T_{\rm M}$ for Ch21 was \approx 83.7°C and for Ch18 was \approx 80.4°C (data not shown). The same PCR protocol was then performed in a dPCR chip on the TEC, and the F images of the dPCR chip were captured at the end of the thermal cycling. Subsequently, the MCA was captured in the range from 70°C to 95°C (Figure 22).

The dPCR chip was loaded using a solution with cn of 1 872, corresponding to the λ value of 0.07 copies partition⁻¹. The results of duplex amplification were not quantified due to the amplification defects on the dPCR chip. However, the MATLAB algorithm for image analysis of dPCR duplexing method by capturing a fluorescent image of the dPCR chip at various temperatures is optimized and prepared for multiplex quantification. The quantification is based on histogram building as shown above, with the

difference that the histograms of occurrence as a function of fluorescent intensity are extracted at different temperatures [80].

The MCA results were processed by MATLAB-based script introduced above. A few melting curves from six partitions (marked in Figure 22) for female genomic DNA are shown in Figure 23A and its – dF/dT in Figure 23B. The T_M^* of Ch21 was determined at ≈83.3°C and ≈80.2°C for Chr18. Therefore, the fluorescent signal from the red microwells could not be identified at 81°C and higher, as it was over the T_M of the Chr18. The blue microwells exhibited an adequate fluorescence signal at a temperature of 83°C. However, with the increased temperature, its fluorescence dropped, and over 85°C, neither of the two amplicons could be identified as dsDNA molecules melted into the ssDNA. The difference between qPCR T_M and T_M^* was only ≈0.4°C for Ch21 and ≈0.2°C for Chr18. The temperatures deviations between the two PCR platforms are in a good relationship with previous experiments. The assay yielded good PCR efficiency.

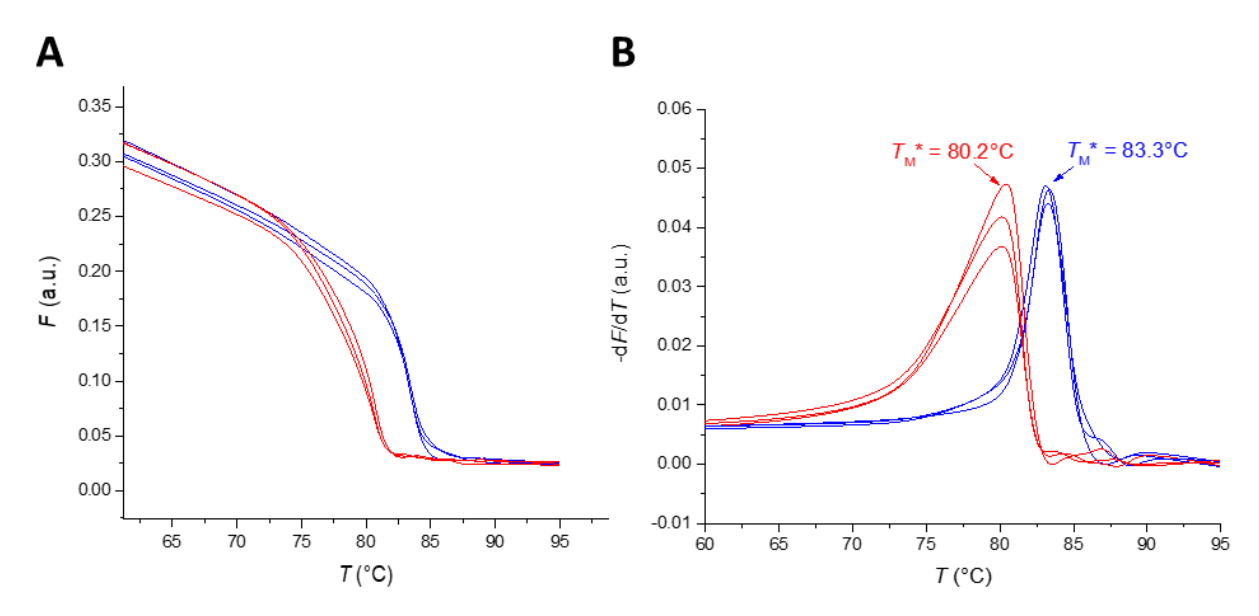


Figure 23 (A) Melting curves from six microwells for female genomic DNA, containing target genes Chr21 (blue curves) and Chr18 (red curves) in the ratio 1:1 after dPCR and (B) their –d*F*/d*T* values.

A single fluorescent channel-based PCR multiplexing method was proposed to qualitatively detect dengue fever serotype [36] or *Vibrio cholerae* [35] at the end of thermal cycling. It was either based on different lengths of amplicons distinguished by electrophoresis or MCA of an amplicon after the PCR, with each target having a different $T_{\rm M}$. The single channel multiplex PCR was then extended using CFM from qualitative to quantitative by performing MCA during each PCR cycle to detect concurrently two [20] or three [18] amplicons (chapter 1.1.1.2). Then simplified technique capable of detecting two amplicons by a combination of FAM probe specific to the one amplicon in the presence of a nonspecific EvaGreen intercalating dye was introduced [33] and later further analyzed [34].

A few techniques use single fluorescent channel-based dPCR multiplexing, such as amplicon-size multiplexing [81]. The amplicons are distinguished from each other using their different fluorescence amplitude caused by their different length with image capturing of a cdPCR chip at room temperature. The simultaneous dPCR amplification of two targets detected in a single fluorescence channel using the combination of a FAM labeled probe specific to one target and nonspecific dye EvaGreen, which was intercalated to both target genes, was tested by our group. The method results will be published soon.

More complex multiplexing is based on capturing images of the cdPCR chip at different temperatures and then analyzing MCAs from individual wells using digital high-resolution MCA. This method was utilized for Kirsten rat sarcoma virus genotyping [17] and *Listeria monocytogenes* detection [38]. One of the main advantages of single fluorescent channel-based multiplexing in dPCR is that it greatly simplifies optical detection compared to the probe-based method, as only a single-color optical channel is required. However, fluorescence from non-specific products, such as primer dimers, affects the accuracy of end-point quantification.

2.2 Summary

The key chip dPCR technology was developed. The silicon chips with 26 448 microwells with the volume of one microwell 59 pL were tested for a suitable sampling method. The optimized protocol of sample loading was developed with respect to eliminating amplification defects. The dPCR chip was filled with the 4 μ L of PCR master mix, covered with 10 μ L of mineral oil, and the modified covered glass. The loaded dPCR chips with various target DNAs were amplified and subsequently quantified. The proposed image-to-answer algorithm for dPCR image processing automatically locates the partitions, extracts a fluorescent signal, and analyzes it. It includes two major parts: extraction of partition locations and subsequent fluorescent signal analysis. The dPCR chips proved their potential to amplify synthetic DNA and isolated HBV and female genomic DNA. The experimental results of quantification reported significant error between the input and calculated λ values. Imperfect loading of the sample to the chip and some evaporation during thermal cycling led to deviations of quantification.

However, the very uniform temperature distribution on the dPCR chip was obtained by MCA-based temperature determination at the dPCR chip surface [41]. The method offered a specific, precise, and photobleaching independent method of $T_{\rm M}$ measurement to calibrate the system temperature sensor with respect to the liquid inside the dPCR chip partitions. It was not affected by the heat capacitance of the temperature probe or the small sample size as with traditional temperature sensors. The presented method digitally defined the temperature fluctuation of each partition at the dPCR chip surface and obtained the overall distribution of the temperature profile.

Finally, the duplex dPCR method capturing a fluorescent image of the dPCR chip at various temperatures using a single fluorescent channel was demonstrated. The target genes Chr21 and Ch18 in the presence of EvaGreen intercalating dye were distinguished from each other based on their extracted melting temperatures. The capabilities of the cdPCR platform were presented with notable results. The improvement of some features is required and will be implemented in the future.

3 Conclusion and future outlooks

dPCR has the potential not only to replace the "gold standard" qPCR but also significantly help in the field of point-of-care analysis. Hence, researchers are trying to improve the dPCR technique and bring it closer to most biomolecular laboratories. The amplification of all target DNA fragments by dPCR relies on many factors such as stability and biocompatibility of PCR reagents with microfluidics, method of partitioning and detection, concentration, and combination of fluorescent detection chemistry or PCR conditions. Thus, higher integration of sampling, thermocycling, and readout is needed to simplify these requirements. Novel dPCR technologies should be able to do an automated analysis by removing the need for postreaction manipulation. Complete laboratory workflow has to provide precise control of sampling, resulting in reducing reagent consumption as well as increasing the number of partitions. After partitioning, the thermal cycling of a sample without liquid transfer step is necessary, eliminating material loss or cross-contamination, following automatic fluorescence readout and analysis of target of interest in a background of a different gene. In laboratories with limited infrastructures and resources, multiplexing using dPCR systems with these features will be appreciated.

The goal of the doctoral thesis was to demonstrate the accessible dPCR technology that implements the simple operation of the device with new architecture, a surface treatment method, and a new sample loading method than currently available dPCR systems. The development was divided into two main parts: (1) development and validation of a droplet qPCR with its detection system and (2) dPCR system. The individual tasks starting with the droplet qPCR development following dPCR chip fabrication with instrumentation, capturing the fluorescent image and its processing, and optimizing the dPCR method for applications were achieved.

One of the purposes was to propose dPCR technology that will expand to the miniaturized and portable platform, thus enlarging its use in local clinics. The following tasks for future work will be aimed to achieve this goal. Future outlooks will focus on performing more measurements with different DNA sample dilutions to determine the limit of detection and the sensitivity of the developed dPCR platform. Then, the platform could be compared with the other experimental or commercial ones. More duplex or even multiplexing with three genes employing dPCR will be performed. The MATLAB algorithm will be applied for multiplex quantification based on analyzing the MCA from each microwell. Moreover, imaging at higher magnification would make the image processing more precise. There is certainly room for an improvement to utilize more pixels, such as a 2× optical magnifier or smaller CMOS imager. The higher magnification could allow to analyze the chips with a higher number of micopartitions, owning smaller partitions diameters. Once these challenging tasks will be completed, the developed dPCR technology could be transformed into the miniaturized and portable dPCR. The purpose would be achieved by employing the smartphone to control the thermal cycling together with the analysis of the results. The simple microfabricated portable technology will offer a low cost, robust and user-friendly detection system. The miniaturized dPCR platform will meet the requirements for POC applications.

References

- [1] D. A. Jonas, I. Elmadfa, K. H. Engel, K. J. Heller, G. Kozianowski, A. König, et al., "Safety Considerations of DNA in Food," *Annals of Nutrition and Metabolism*, vol. 45, pp. 235-254, 2001.
- [2] H. Zhu, H. Zhang, Y. Xu, S. Laššáková, M. Korabečná, and P. Neužil, "PCR past, present and future," *BioTechniques*, vol. 69, pp. 317-325, 2020.
- [3] K. Mullis, F. Faloona, S. Scharf, R. Saiki, G. Horn, and H. Erlich, "Specific Enzymatic Amplification of DNA Invitro The Polymerase Chain-Reaction," *Cold Spring Harbor Symposia on Quantitative Biology*, vol. 51, pp. 263–273, 1986.
- [4] L. Cao, X. Cui, J. Hu, Z. Li, J. R. Choi, Q. Yang, *et al.*, "Advances in digital polymerase chain reaction (dPCR) and its emerging biomedical applications," *Biosensors and Bioelectronics*, vol. 90, pp. 459-474, 2017.
- [5] B. Vogelstein and K. W. Kinzler, "Digital PCR," *Proceedings of the National Academy of Sciences of the United States of America*, vol. 96, pp. 9236-9241, 1999.
- [6] J. Pavšič, J. Žel, and M. Milavec, "Assessment of the real-time PCR and different digital PCR platforms for DNA quantification," *Analytical and Bioanalytical Chemistry*, vol. 408, pp. 107-121, 2016.
- [7] M. Gaňová, H. Zhang, H. Zhu, M. Korabečná, and P. Neužil, "Multiplexed digital polymerase chain reaction as a powerful diagnostic tool," *Biosensors and Bioelectronics*, vol. 181, p. 113155, 2021.
- [8] *Molecular Diagnostics Market Size & Share Report, 2021-2028.* Available: https://www.grandviewresearch.com/industry-analysis/molecular-diagnostics-market, 2020.
- [9] H. Zhu, P. Podesva, X. Liu, H. Zhang, T. Teply, Y. Xu, et al., "IoT PCR for pandemic disease detection and its spread monitoring," *Sensors and Actuators B: Chemical*, vol. 303, p. 127098, 2020.
- [10] C. D. Ahrberg, B. R. Ilic, A. Manz, and P. Neužil, "Handheld real-time PCR device," *Lab on a Chip*, vol. 16, pp. 586-592, 2016.
- [11] P. Neuzil, L. Novak, J. Pipper, S. Lee, L. F. P. Ng, and C. Zhang, "Rapid detection of viral RNA by a pocket-size real-time PCR system," *Lab on a Chip*, vol. 10, pp. 2632-2634, 2010.
- [12] C. D. Ahrberg, A. Manz, and P. Neužil, "Palm-Sized Device for Point-of-Care Ebola Detection," *Analytical Chemistry*, vol. 88, pp. 4803-4807, 2016.
- [13] W. J. G. Melchers, J. Kuijpers, J. J. Sickler, and J. Rahamat-Langendoen, "Lab-in-a-tube: Real-time molecular point-of-care diagnostics for influenza A and B using the cobas® Liat® system," *Journal of Medical Virology,* vol. 89, pp. 1382-1386, 2017.
- [14] H. Yang, Z. Chen, X. Cao, Z. Li, S. Stavrakis, J. Choo, *et al.*, "A sample-in-digital-answer-out system for rapid detection and quantitation of infectious pathogens in bodily fluids," *Analytical and Bioanalytical Chemistry*, vol. 410, pp. 7019-7030, 2018.
- [15] N. Kanwar, J. Michael, K. Doran, E. Montgomery, and R. Selvarangan, "Comparison of the ID Now Influenza A & B 2, Cobas Influenza A/B, and Xpert Xpress Flu Point-of-Care Nucleic Acid Amplification Tests for Influenza A/B Virus Detection in Children," *Journal of Clinical Microbiology*, vol. 58, 2020.

- [16] T. Gou, J. Hu, W. Wu, X. Ding, S. Zhou, W. Fang, *et al.*, "Smartphone-based mobile digital PCR device for DNA quantitative analysis with high accuracy," *Biosensors and Bioelectronics*, vol. 120, pp. 144-152, 2018.
- [17] J. Tanaka, T. Nakagawa, A. Shiratori, Y. Shimazaki, C. Uematsu, M. Kamahori, *et al.*, "KRAS genotyping by digital PCR combined with melting curve analysis," *Scientific Reports*, vol. 9, p. 2626, 2019.
- [18] H. Zhang, M. Gaňová, Z. Yan, H. Chang, and P. Neužil, "PCR Multiplexing Based on a Single Fluorescent Channel Using Dynamic Melting Curve Analysis," *ACS Omega*, vol. 5, pp. 30267-30273, 2020.
- [19] H. Zhang, H. Li, H. Zhu, J. Pekárek, P. Podešva, H. Chang, et al., "Revealing the secrets of PCR," Sensors and Actuators B: Chemical, vol. 298, p. 126924, 2019.
- [20] C. D. Ahrberg, A. Manz, and P. Neuzil, "Single Fluorescence Channel-based Multiplex Detection of Avian Influenza Virus by Quantitative PCR with Intercalating Dye," *Scientific Reports*, vol. 5, p. 11479, 2015.
- [21] J. K. Rockstroh, "Influence of viral hepatitis on HIV infection," *Journal of Hepatology*, vol. 44, pp. S25-S27, 2006.
- [22] J. R. Barbosa, J. K. B. Colares, G. L. Flores, V. F. Cortes, J. C. Miguel, M. M. Portilho, *et al.*, "Performance of rapid diagnostic tests for detection of Hepatitis B and C markers in HIV infected patients," *Journal of Virological Methods*, vol. 248, pp. 244-249, 2017.
- [23] A. P. Kourtis, M. Bulterys, D. J. Hu, and D. J. Jamieson, "HIV-HBV coinfection—A global challenge," *New England Journal of Medicine*, vol. 366, pp. 1749-1752, 2012.
- [24] D. Frentz, A. M. Wensing, J. Albert, D. Paraskevis, A. B. Abecasis, O. Hamouda, *et al.*, "Limited cross-border infections in patients newly diagnosed with HIV in Europe," *Retrovirology*, vol. 10, pp. 1-10, 2013.
- [25] M. K. Akmatov, R. T. Mikolajczyk, R. Krumkamp, T. Wörmann, J. J. Chu, G. Paetzelt, *et al.*, "Availability of indicators of migration in the surveillance of HIV, tuberculosis and hepatitis B in the European Union—a short note," *Journal of Public Health*, vol. 20, pp. 483-486, 2012.
- [26] P. Schlagenhauf, F. Santos-O'Connor, and P. Parola, "The practice of travel medicine in Europe," *Clinical Microbiology and Infection*, vol. 16, pp. 203-208, 2010.
- [27] P. Markoulatos, N. Siafakas, and M. Moncany, "Multiplex polymerase chain reaction: a practical approach," *Journal of Clinical Laboratory Analysis*, vol. 16, pp. 47-51, 2002.
- [28] A. Iwobi, D. Sebah, I. Kraemer, C. Losher, G. Fischer, U. Busch, *et al.*, "A multiplex real-time PCR method for the quantification of beef and pork fractions in minced meat," *Food Chemistry*, vol. 169, pp. 305-313, 2015.
- [29] T. Ishige, S. Murata, T. Taniguchi, A. Miyabe, K. Kitamura, K. Kawasaki, *et al.*, "Highly sensitive detection of SARS-CoV-2 RNA by multiplex rRT-PCR for molecular diagnosis of COVID-19 by clinical laboratories," *Clinica Chimica Acta*, vol. 507, pp. 139-142, 2020.
- [30] D. K. Geetha, B. Sivaraman, R. Rammohan, N. Venkatapathy, and P. S. Ramatchandirane, "A SYBR Green based multiplex Real-Time PCR assay for rapid detection and differentiation of ocular bacterial pathogens," *Journal of Microbiological Methods*, vol. 171, p. 105875, 2020.
- [31] M. E. Ali, M. A. Razzak, S. B. Abd Hamid, M. M. Rahman, M. Al Amin, and N. R. Abd Rashid, "Multiplex PCR assay for the detection of five meat species forbidden in Islamic foods," *Food Chemistry*, vol. 177, pp. 214-224, 2015.

- [32] S.-M. Suh, M.-J. Kim, H.-I. Kim, H.-J. Kim, and H.-Y. Kim, "A multiplex PCR assay combined with capillary electrophoresis for the simultaneous detection of tropomyosin allergens from oyster, mussel, abalone, and clam mollusk species," *Food Chemistry*, vol. 317, p. 126451, 2020.
- [33] C. D. Ahrberg and P. Neužil, "Doubling throughput of a real-time PCR," *Scientific Reports*, vol. 5, pp. 1-9, 2015.
- [34] H. Zhang, Z. Yan, X. Wang, M. Gaňová, H. Chang, S. Laššáková, *et al.*, "Determination of Advantages and Limitations of qPCR Duplexing in a Single Fluorescent Channel," *ACS Omega*, vol. 6, pp. 22292-22300, 2021.
- [35] A. J. Gubala, "Multiplex real-time PCR detection of Vibrio cholerae," *Journal of Microbiological Methods*, vol. 65, pp. 278-293, 2006.
- [36] E. Harris, T. G. Roberts, L. Smith, J. Selle, L. D. Kramer, S. Valle, *et al.*, "Typing of dengue viruses in clinical specimens and mosquitoes by single-tube multiplex reverse transcriptase PCR," *Journal of Clinical Microbiology*, vol. 36, pp. 2634-2639, 1998.
- [37] C. T. Wittwer, M. G. Herrmann, A. A. Moss, and R. P. Rasmussen, "Continuous fluorescence monitoring of rapid cycle DNA amplification," *BioTechniques*, vol. 22, pp. 130-138, 1997.
- [38] D. O. Velez, H. Mack, J. Jupe, S. Hawker, N. Kulkarni, B. Hedayatnia, *et al.*, "Massively parallel digital high resolution melt for rapid and absolutely quantitative sequence profiling," *Scientific Reports*, vol. 7, p. 42326, 2017.
- [39] A. Moniri, J. Rodriguez-Manzano, K. Malpartida-Cardenas, L.-S. Yu, X. Didelot, A. Holmes, *et al.*, "Framework for dna quantification and outlier detection using multidimensional standard curves," *Analytical Chemistry*, vol. 91, pp. 7426-7434, 2019.
- [40] J. Rodriguez-Manzano, A. Moniri, K. Malpartida-Cardenas, J. Dronavalli, F. Davies, A. Holmes, *et al.*, "Simultaneous single-channel multiplexing and quantification of carbapenem-resistant genes using multidimensional standard curves," *Analytical Chemistry*, vol. 91, pp. 2013-2020, 2019.
- [41] M. Gaňová, X. Wang, Z. Yan, H. Zhang, T. Lednický, M. Korabečná, *et al.*, "Temperature non-uniformity detection on dPCR chips and temperature sensor calibration," *RSC Advances*, vol. 12, pp. 2375-2382, 2022.
- [42] L. Malic, J. Daoud, M. Geissler, A. Boutin, L. Lukic, M. Janta, et al., "Epigenetic subtyping of white blood cells using a thermoplastic elastomer-based microfluidic emulsification device for multiplexed, methylation-specific digital droplet PCR," *Analyst*, vol. 144, pp. 6541-6553, 2019.
- [43] A. S. Basu, "Digital Assays Part I: Partitioning Statistics and Digital PCR," *SLAS Technology: Translating Life Sciences Innovation*, vol. 22, pp. 369-386, 2017.
- [44] R. M. Ripken, S. Schlautmann, R. G. Sanders, J. G. Gardeniers, and S. Le Gac, "Monitoring phase transition of aqueous biomass model substrates by high-pressure and high-temperature microfluidics," *Electrophoresis*, vol. 40, pp. 563-570, 2019.
- [45] Y. Matsubara, K. Kerman, M. Kobayashi, S. Yamamura, Y. Morita, Y. Takamura, *et al.*, "Onchip nanoliter-volume multiplex TaqMan polymerase chain reaction from a single copy based on counting fluorescence released microchambers," *Analytical Chemistry*, vol. 76, pp. 6434-6439, 2004.
- [46] J. Khandurina, T. E. McKnight, S. C. Jacobson, L. C. Waters, R. S. Foote, and J. M. Ramsey, "Integrated System for Rapid PCR-Based DNA Analysis in Microfluidic Devices," *Analytical Chemistry*, vol. 72, pp. 2995-3000, 2000.

- [47] V. Miralles, A. Huerre, F. Malloggi, and M.-C. Jullien, "A Review of Heating and Temperature Control in Microfluidic Systems: Techniques and Applications," *Diagnostics (Basel, Switzerland)*, vol. 3, pp. 33-67, 2013.
- [48] K. R. Sreejith, C. H. Ooi, J. Jin, D. V. Dao, and N.-T. Nguyen, "Digital polymerase chain reaction technology–recent advances and future perspectives," *Lab on a Chip*, vol. 18, pp. 3717-3732, 2018.
- [49] C. D. Ahrberg, J. W. Choi, J. M. Lee, K. G. Lee, S. J. Lee, A. Manz, et al., "Plasmonic heating-based portable digital PCR system," *Lab on a Chip*, vol. 20, pp. 3560-3568, 2020.
- [50] H. Nagai, Y. Murakami, K. Yokoyama, and E. Tamiya, "High-throughput PCR in silicon based microchamber array," *Biosensors and Bioelectronics*, vol. 16, pp. 1015-1019, 2001.
- [51] T.-M. Hsieh, C.-H. Luo, F.-C. Huang, J.-H. Wang, L.-J. Chien, and G.-B. Lee, "Enhancement of thermal uniformity for a microthermal cycler and its application for polymerase chain reaction," *Sensors and Actuators B: Chemical*, vol. 130, pp. 848-856, 2008.
- [52] P.-L. Quan, M. Sauzade, and E. Brouzes, "dPCR: A Technology Review," *Sensors*, vol. 18, p. 1271, 2018.
- [53] E. T. Lagally, P. C. Simpson, and R. A. Mathies, "Monolithic integrated microfluidic DNA amplification and capillary electrophoresis analysis system," *Sensors and Actuators B: Chemical*, vol. 63, pp. 138-146, 2000.
- [54] C.-Y. Lee, G.-B. Lee, H.-H. Liu, and F.-C. Huang, "MEMS-based temperature control systems for DNA amplification," *International Journal of Nonlinear Sciences and Numerical Simulation*, vol. 3, pp. 215-218, 2002.
- [55] Y. Wang, Q. Zhang, R. Tao, D. Chen, J. Xie, H. Torun, et al., "A rapid and controllable acoustothermal microheater using thin film surface acoustic waves," *Sensors and Actuators A: Physical*, vol. 318, p. 112508, 2021.
- [56] L. Gerdes, A. Iwobi, U. Busch, and S. Pecoraro, "Optimization of digital droplet polymerase chain reaction for quantification of genetically modified organisms," *Biomolecular Detection and Quantification*, vol. 7, pp. 9-20, 2016.
- [57] S. Ni, Y. Bu, H. Zhu, P. Neuzil, and L. Yobas, "A Sub-nL Chip Calorimeter and Its Application to the Measurement of the Photothermal Transduction Efficiency of Plasmonic Nanoparticles," *Journal of Microelectromechanical Systems*, vol. 30, pp. 759-769, 2021.
- [58] P. Neuzil, F. Cheng, J. B. W. Soon, L. L. Qian, and J. Reboud, "Non-contact fluorescent bleaching-independent method for temperature measurement in microfluidic systems based on DNA melting curves," *Lab on a Chip,* vol. 10, pp. 2818-2821, 2010.
- [59] S. Ni, H. Zhu, P. Neuzil, and L. Yobas, "A SiN Microcalorimeter and a Non-Contact Precision Method of Temperature Calibration," *Journal of Microelectromechanical Systems*, vol. 29, pp. 1103-1105, 2020.
- [60] D. A. Selck and R. F. Ismagilov, "Instrument for real-time digital nucleic acid amplification on custom microfluidic devices," *PLOS One*, vol. 11, p. e0163060, 2016.
- [61] H. Yin, Z. Wu, N. Shi, Y. Qi, X. Jian, L. Zhou, *et al.*, "Ultrafast multiplexed detection of SARS-CoV-2 RNA using a rapid droplet digital PCR system," *Biosensors and Bioelectronics*, vol. 188, p. 113282, 2021.
- [62] Y. Ho Kim, I. Yang, Y.-S. Bae, and S.-R. Park, "Performance evaluation of thermal cyclers for PCR in a rapid cycling condition," *BioTechniques*, vol. 44, pp. 495-505, 2008.

- [63] C. Shen and C. Gau, "Thermal chip fabrication with arrays of sensors and heaters for microscale impingement cooling heat transfer analysis and measurements," *Biosensors and Bioelectronics*, vol. 20, pp. 103-114, 2004.
- [64] M. W. Khalid, C. Whitehouse, R. Ahmed, M. U. Hassan, and H. Butt, "Remote Thermal Sensing by Integration of Corner-Cube Optics and Thermochromic Materials," *Advanced Optical Materials*, vol. 7, p. 1801013, 2019.
- [65] P. Neužil, W. Sun, T. Karásek, and A. Manz, "Nanoliter-sized overheated reactor," *Applied Physics Letters*, vol. 106, p. 024104, 2015.
- [66] C. Tan, X. Chen, F. Wang, D. Wang, Z. Cao, X. Zhu, et al., "A multiplex droplet digital PCR assay for non-invasive prenatal testing of fetal aneuploidies," *Analyst*, vol. 144, pp. 2239-2247, 2019.
- [67] J. F. Huggett, S. Cowen, and C. A. Foy, "Considerations for digital PCR as an accurate molecular diagnostic tool," *Clinical Chemistry*, vol. 61, pp. 79-88, 2015.
- [68] J. F. Huggett, C. A. Foy, V. Benes, K. Emslie, J. A. Garson, R. Haynes, *et al.*, "The Digital MIQE Guidelines: Minimum Information for Publication of Quantitative Digital PCR Experiments," *Clinical Chemistry*, vol. 59, pp. 892-902, 2013.
- [69] B. K. Jacobs, E. Goetghebeur, and L. Clement, "Impact of variance components on reliability of absolute quantification using digital PCR," *BMC Bioinformatics*, vol. 15, pp. 1-13, 2014.
- [70] Z. Yan, H. Zhang, X. Wang, M. Ganova, T. Lednicky, H. Zhu, et al., "An image-to-answer algorithm for fully automated digital PCR image processing," *Lab on a Chip*, 2022.
- [71] A. Aralar, Y. Yuan, K. Chen, Y. Geng, D. O. Velez, M. Sinha, *et al.*, "Improving Quantitative Power in Digital PCR through Digital High-Resolution Melting," *Journal of Clinical Microbiology*, vol. 58, pp. e00325-20, 2020.
- [72] Z. Hu, W. Fang, T. Gou, W. Wu, J. Hu, S. Zhou, et al., "A novel method based on a Mask R-CNN model for processing dPCR images," *Analytical Methods*, vol. 11, pp. 3410-3418, 2019.
- [73] Z. Beini, C. Xuee, L. Bo, and W. Weijia, "A New Few-Shot Learning Method of Digital PCR Image Detection," *IEEE Access*, vol. 9, pp. 74446-74453, 2021.
- [74] N. Majumdar, T. Wessel, and J. Marks, "Digital PCR modeling for maximal sensitivity, dynamic range and measurement precision," *PLOS One*, vol. 10, p. e0118833, 2015.
- [75] M. Krishnan, D. T. Burke, and M. A. Burns, "Polymerase Chain Reaction in High Surface-to-Volume Ratio SiO2 Microstructures," *Analytical Chemistry*, vol. 76, pp. 6588-6593, 2004.
- [76] O. Henegariu, N. Heerema, S. Dlouhy, G. Vance, and P. Vogt, "Multiplex PCR: critical parameters and step-by-step protocol," *BioTechniques*, vol. 23, pp. 504-511, 1997.
- [77] J. Quick, N. D. Grubaugh, S. T. Pullan, I. M. Claro, A. D. Smith, K. Gangavarapu, *et al.*, "Multiplex PCR method for MinION and Illumina sequencing of Zika and other virus genomes directly from clinical samples," *Nature protocols*, vol. 12, pp. 1261-1276, 2017.
- [78] I. Y. Iourov, S. G. Vorsanova, T. Liehr, and Y. B. Yurov, "Aneuploidy in the normal, Alzheimer's disease and ataxia-telangiectasia brain: differential expression and pathological meaning," *Neurobiology of Disease*, vol. 34, pp. 212-220, 2009.
- [79] M. A. Hultén, J. Jonasson, A. Nordgren, and E. Iwarsson, "Germinal and somatic trisomy 21 mosaicism: how common is it, what are the implications for individual carriers and how does it come about?," *Current Genomics*, vol. 11, pp. 409-419, 2010.

- [80] H. Zhang, Z. Yan, X. Wang, M. Gaňová, M. Korabečná, P. Zahradník, *et al.*, "Digital PCR system development accelerator—A methodology to emulate dPCR results," *Sensors and Actuators B: Chemical*, vol. 358, p. 131527, 2022.
- [81] T. Demeke and D. Dobnik, "Critical assessment of digital PCR for the detection and quantification of genetically modified organisms," *Analytical and Bioanalytical Chemistry*, vol. 410, pp. 4039-4050, 2018.

Publications

M. Gaňová, X. Wang, Z. Yan, H. Zhang, T. Lednický, M. Korabečná, *et al.*, "Temperature non-uniformity detection on dPCR chips and temperature sensor calibration," *RSC Advances*, vol. 12, pp. 2375-2382, 2022.

My contribution: design of experiments, sample preparation, measurements and experiment analysis, writing the manuscript.

- **M. Gaňová**, H. Zhang, H. Zhu, M. Korabečná, and P. Neužil, "Multiplexed digital polymerase chain reaction as a powerful diagnostic tool," *Biosensors and Bioelectronics*, vol. 181, p. 113155, 2021. *My contribution:* writing the part of manuscript.
- H. Zhang, **M. Gaňová**, Z. Yan, H. Chang, and P. Neužil, "PCR Multiplexing Based on a Single Fluorescent Channel Using Dynamic Melting Curve Analysis," *ACS Omega*, vol. 5, pp. 30267-30273, 2020.

My contribution: measurements and experiment analysis, writing the manuscript.

H. Zhang, Z. Yan, X. Wang, **M. Gaňová**, H. Chang, S. Laššáková, *et al.*, "Determination of Advantages and Limitations of qPCR Duplexing in a Single Fluorescent Channel," *ACS Omega*, vol. 6, pp. 22292-22300, 2021.

My contribution: manuscript revision.

H. Zhang, Z. Yan, X. Wang, **M. Gaňová**, M. Korabečná, P. Zahradník, *et al.*, "Digital PCR system development accelerator—A methodology to emulate dPCR results," *Sensors and Actuators B: Chemical*, vol. 358, p. 131527, 2022.

My contribution: experiments analysis, validation, manuscript revision.

Z. Yan, H. Zhang, X. Wang, **M. Gaňová**, T. Lednický, H. Zhu, X. Liu, M. Korabečná, H. Chang, P. Neužil, "An image-to-answer algorithm for fully automated digital PCR image processing," *Lab on Chip*, 2022. *My contribution:* design of experiments, sample preparation, measurements with dPCR chip of 50 μm well diameter, manuscript revision.

SUBMITTED PUBLICATIONS

H. Zhang, S. Laššáková, Z. Yan, X. Wang, **M**. **Gaňová**, H. Chang, M. Korabečná, P. Neužil, "dPCR duplexing method in a single fluorescence channel," *Analytica Chimica Acta*. *My contribution:* manuscript revision.

CONFERENCES CONTRIBUTIONS

Oral presentations:

- **M. Gaňová**, T. Lednický, P. Neužil, "The determination of DNA melting temperature by microchip digital polymerase chain reaction," *Ceitec Ph.D. Retreat 2021-Abstracts*, First Edition, p. 24-24, 2021.
- **M. Gaňová**, T. Lednický, Z. Yan, P. Neužil, "The optimization of microchip digital polymerase chain reaction (dPCR) with microwell sample dispersion," *Nanocon 2021-Abstracts*, 1. Edition, p.45-45, ISBN: 978-80-88365-00-6, 2021.



Figure 24 My talk was awarded by honorable mention for the author of the lecture for up to 33 years.

Poster presentations:

- **M. Gaňová**, P. Neužil, "Development of digital polymerase chain reaction," *European Biotechnology Congress*, Biotechnology and Biotechnological Equipment, Abstracts, Abingdon: Taylor & Francis Ltd, p. S62, ISSN: 1314-3530, 2020.
- **M. Gaňová**, P. Neužil, "Droplet real-time PCR and microchip-based digital PCR technology in one device," *Nanocon 2019-Abstracts*, 1. Edition, p. 121-122, ISBN: 978-80-87294-94-9, 2019.